Title

- Highly efficient and low-cost single-cell culture platform for unbiased analysis of human memory B cell repertoire and antibody discovery

- Short title: *Streamlined, low-cost antibody discovery platform*

Authors

Luciana Conde [1,2,#], Debora L. Oliveira[1,#], Gabriela Maciel[1], Fernando Castro[1], Aline de Oliveira Albuquerque[3], Danielle A.S. Rodrigues[1], Yare Mëllo[1], Gustavo Meira de Assis[1,4], Bárbara Gabrielle[1], Suyane S. Ferreira[5], Marcela S. Cunha[5], Carlena Navas[6], Manuela C. Emiliano[6], Marcele N. Rocha[6], Barbara Soares[7], Lucas Tostes[1], Philippe Caloba[1], Bruno Maia[5], Francisco M. Bastos de Oliveira[7], Amilcar Tanuri[8], Orlando C. Ferreira Jr.[8], Terezinha M.P.P. Castineiras[9], João Hermínio Martins da Silva[3], Juliana Echevarria[5], Marcelo Bozza[5], Leda R. Castilho[10], Luciana J. da Costa[5,9], Liza F. Felicori[6], Alberto Nobrega[5], Gabriel Victora[4,11], Carolina Lucas[2], Adriana Bonomo[12], André M. Vale[1,*]

Affiliations

[1] Laboratório de Biologia de Linfócitos, Instituto de Biofísica Carlos Chagas Filho, Universidade Federal do Rio de Janeiro, Rio de Janeiro, RJ, Brazil.
[2] Department of Immunobiology, Yale University School of Medicine, New Haven, CT, USA
[3] Fundação Oswaldo Cruz. FIOCRUZ Ceará. Eusébio, CE, Brazil.
[4] Laboratory of Lymphocyte Dynamics, The Rockefeller University, New York, NY, USA
[5] Instituto de Microbiologia Paulo de Góes, Universidade Federal do Rio de Janeiro, Rio de Janeiro, RJ, Brazil.
[6] Laboratory of Synthetic Biology and Biomimetics, Departamento de Bioquímica e Imunologia, Instituto de Ciências Biológicas - ICB, Universidade Federal de Minas Gerais, Belo Horizonte, MG, Brazil
[7] Laboratório de Imunoreceptores e Sinalização, Instituto de Biofísica Carlos Chagas Filho, Universidade Federal do Rio de Janeiro, Rio de Janeiro, RJ, Brazil.
[8] Laboratório de Virologia Molecular, Departamento de Genética, Instituto de Biologia, Universidade Federal do Rio de Janeiro, Rio de Janeiro, RJ, Brasil
[9] Núcleo de Enfrentamento e Estudos de Doenças Infecciosas Emergentes e Reemergentes, Universidade Federal do Rio de Janeiro, Rio de Janeiro, RJ, Brasil
[10] Laboratório de Engenharia de Cultivos Celulares, Programa de Engenharia Química, COPPE, Universidade Federal do Rio de Janeiro, Rio de Janeiro, RJ, Brazil.
[11] Howard Hughes Medical Institute, New York, NY, USA
[12]Thymus Research Laboratory, Fundação Oswaldo Cruz, IOC-FIOCRUZ, Rio de Janeiro, RJ, Brazil
[#]These authors contributed equally to this work.
*Correspondence to André M. Vale: valeam@biof.ufrj.br

Abstract

The SARS-CoV-2 pandemic underscored the need for innovative approaches to study humoral immunity and isolate monoclonal antibodies (mAbs) with diagnostic and therapeutic potential. Current methods for repertoire analysis at the clonal level require large-scale recombinant mAb production, limiting accessibility and delaying functional insight. We developed a single-cell culture (SCC) platform that enables profiling of human memory B cells (MBCs) and direct recovery of functional mAbs. Using samples from COVID-19 convalescent and vaccinated donors, we optimized SCCs with NB21 feeder cells, R848, and IL-2, achieving efficient clonal expansion and antibody secretion in short-term cultures. Screening and pseudovirus neutralization assays were performed directly with culture supernatants, bypassing the need for early recombinant antibody production. Antigen-baited cytometry sorting enriched Spike-specific MBCs by ~30-fold. Among 592 isolated mAbs, 53% bound the Wuhan Spike, targeting the receptor-binding domain (28%), the N-terminal domain (15%), or other regions (57%). Cross-reactivity analysis revealed that 40% of anti-Spike mAbs recognized all tested variants of concern. VH/VL sequencing uncovered convergent rearrangements, including public V3-30 and V3-53/V3-66 clones, consistent with global findings. Two public RBD-specific antibodies demonstrated broad neutralization when produced recombinantly. Together, these results validate the SCC system as a streamlined approach for unbiased repertoire analysis and functional mAb isolation. More broadly, the platform provides a practical framework for linking B cell clonal composition with antigen specificity and serum antibody responses. By reducing costs and simplifying workflows, it expands opportunities for antibody discovery and immuno-epidemiological studies, fostering wider global participation in therapeutic antibody research.

MAIN TEXT

Introduction

The SARS-CoV-2 pandemic, with its high morbidity and mortality rates (1), highlighted the urgent need for new methods to study and monitor humoral immune responses to infection and vaccination at the level of individual B cell clonotypes. During the pandemic, immune escape was driven by the random accumulation of mutations in the viral genome, resulting in the emergence of highly transmissible Variants of Concern (VOCs) and significant antigenic drift in the Spike protein. These mutations, concentrated primarily in the receptor-binding domain (RBD) and the N-terminal domain (NTD), posed challenges to vaccination strategies and emphasized the need to monitor humoral responses in order to identify vaccine-induced cross-reactive and broadly neutralizing antibody responses (2).

Memory B cells (MBCs) are central to long-lasting immunity, generating high-affinity antibodies upon antigen re-encounter. These cells arise during primary antigen exposure and often undergo somatic hypermutation and affinity maturation in germinal centers, enhancing their ability to produce potent antibody responses (3). Upon reactivation, MBCs rapidly differentiate into antibody-secreting plasma cells, enabling efficient and robust secondary responses (4). Given their pivotal role in sustaining immune protection and their significant diversity, particularly against rapidly evolving pathogens, monitoring and analyzing MBC repertoires is a priority (5). This is particularly important for identifying monoclonal antibodies with therapeutic potential.

Single-cell high-throughput repertoire sequencing techniques have revolutionized the study of antibody responses, enabling detailed analyses of clonal evolution, somatic hypermutation, and lineage dynamics (6). These advancements have substantially enhanced our understanding of how diverse and effective antibody responses are generated and maintained. However, current high-throughput repertoire analysis is limited by their inability to simultaneously determine antigen-binding specificities alongside clonotypic variable Ig gene (VDJ/VJ) rearrangements. Presently, characterization of antigen specificity requires the cloning and expression of Ig genes carrying the identified VDJ/VJ rearrangements in cell lines to produce recombinant monoclonal antibodies (mAbs) for antigen-binding screening assays (7). This process is labor-intensive and time-consuming as it involves the production of hundreds recombinant mAbs to pinpoint the desired antibody. These technical demands are further compounded by financial barriers in many research settings, limiting widespread application of such approaches to pandemic and locally relevant pathogens.

In vitro culture methods of human B cells have been previously described as an alternative to the production of recombinant mAbs. A classical protocol described by Pinna et al. (8) requires co-cultures with peripheral blood mononuclear cells (PBMCs) from the same individual to act as feeder cells to support B cell growth. This approach allows the estimation of antigen-specific clonal frequencies and the study of the humoral response at the clonal level. While these cultures can efficiently stimulate single cell clonal expansion, they do not allow for unique recovery of VH/VL rearrangements from growing clones because of mRNA contamination from endogenous B cells in the PBMCs used as feeder cells.

In mouse experimental models, culture protocols employing feeder cell lines expressing activating B cell factors have been established as an efficient system for isolating monoclonal antibodies from naïve, and germinal center B cells (9-11). Similar culture systems have also been described for human B cells (12, 13); however, these protocols are generally more complex and delicate than those used in mice. They often require continuous supplementation with a cocktail of multiple cytokines, and the differentiation of antibody-secreting plasmablasts typically occurs only after 15–20 days in culture, much later than in murine systems.

Here, we describe a novel culture system for human B cell cultures that circumvents these limitations. By integrating elements from previously described single B cell culture protocol for both mouse and human, we developed a streamlined new approach based on the murine NB-21 feeder cell line, supplemented only with IL-2 and R848. This short-term (7-day) culture system yields sufficient amount of secreted Ig for antigen screening assays. It proved to be robust, reproducible, and highly efficient in supporting clonal expansion and Ig production, thereby establishing a platform for functional analysis of the human B cell repertoire. Our approach advances several key aspects of human monoclonal antibody discovery: (i) use of supernatants from short term single-cell cultured (SCCs) of memory B cells for antigen-specific screening, cross-reactivity studies across SARS-CoV-2 VOCs, and virus neutralization assays; (ii) analysis of VDJ/VJ gene usage from mRNA/cDNA derived directly from SCC lysates; (iii) high cloning efficiency that allows for an unbiased description of the antibody repertoire, and (iv) identification of mAbs candidates suitable for scalable recombinant production.

To validate the platform, we applied the SCC system to the study of the humoral response to SARS-CoV-2 infection. The results were consistent with previous landmark studies that employed high-throughput single-cell sequencing and recombinant mAbs production (14). Importantly, the protocol presented here offers a practical and accessible alternative for laboratories in low- and middle-income countries, enabling local health institutions to autonomously conduct critical immunological research and complementary epidemiological studies, as well as develop targeted monoclonal antibody therapies make significant contributions to clinical and global scientific efforts.

Results

Establishing culture conditions for human memory B cell expansion

Our research group pioneered the development of an efficient method for analyzing the mouse B cell repertoire, both for VH/VL rearrangements and antigen specificities, by combining high-efficiency B single-cell cultures (SCC) with RT-PCR for *Ig* variable gene amplification and sequencing (10). This approach relies on murine B cells cultured on S17 stromal cells (15), as feeder cells, in the presence of mitogens such as LPS, CpG, and Pam3Cys, to promote proliferation and differentiation into plasma cells *in vitro*. Following an analogous strategy, we designed a similar system for growing human memory B cells (MBCs) taking advantage of feeder cells able to provide essential factors for human B cell proliferation and antibody secretion.

To identify the most efficient feeder cell line for human MBC culture, we tested three previously described feeder cell lines: S17, 40LB, and NB21. S17, a mouse bone marrow stromal cell line which supports myelopoiesis and B lymphopoiesis. 40LB, derived from the 3T3 fibroblast lineage and engineered to express CD40L and BAFF, mimicking germinal center conditions (9). NB21, a derivative of 40LB, further engineered to express IL-21, enhancing mouse B cell survival and Ig secretion (16). To compare the performance of the different feeder cell types, sorted memory B cells (MBCs) from a healthy donor, seronegative donor for SARS-CoV-2 antibodies, were cultured in a limiting dilution assay (LDA) at varying cell densities, and the frequency of immunoglobulin-secreting cells were quantified after 7 days by ELISA. Applying the Poisson distribution, we calculated the frequency of clonable MBCs, defined as the seeding density at which 37% of cultures were negative for antibody detection. NB21 cells demonstrated significantly higher cloning efficiency, outperforming S17 and 40LB feeder lines by at least fourfold (**Supplementary Figures 1A, 1B**).

We confirmed that LPS was ineffective for stimulating human B cells, consistent with previous reports. Instead, optimal conditions for human MBC proliferation required R848 or CpG in combination with high doses of IL-2 (1,000 U/mL), as demonstrated by Pinna et al (2009) (8). Using NB21 as feeder cell, we compared R848 and CpG (both in the presence of hrIL-2) at concentrations of 2 µg/ml and 10nM, respectively. No significant differences in their efficacy to support memory B cell proliferation and antibody production were observed (**Supplementary Figure 1C**). Therefore, R848 was chosen for further experiments due to its cost-effectiveness and dual role as a TLR7 and TLR8 agonist (17).

Recognizing the need for methods adaptable to low-resource settings, we compared manual cell plating with automated robotic plating integrated into the sorting device. Both approaches yielded similar frequencies of responding B cells, with a representative experiment indicating 55% and 59% responder frequencies for robotic and manual plating, respectively (**Supplementary Figure 1D**).

Validation of a culture system for comprehensive and unbiased MBC profiling

LDA using culture systems on efficient feeder cells enable reliable quantification of responding B cells (18, 19). We therefore applied this methodology to analyze the Spike-specific MBC repertoire in SARS-CoV-2-exposed donors and convalescent patients, with samples collected in 2020, before COVID-19 vaccination became available. SARS-CoV2-

185 exposed donors were healthcare workers who had direct contact with patients, remained
186 asymptomatic, and tested negative for SARS-CoV-2 by weekly PCR screening. These
187 experiments aimed to assess the sensitivity and potential of our system for detecting and
188 characterizing antigen-specific B cell responses.

189 We first assessed antibody titers of anti-SARS-CoV-2 Spike IgG in sera from two
190 cohorts: (1) SARS-CoV2-exposed donors, and (2) convalescent patients from 2020.
191 Additionally, as a control, we included 23 pre-COVID samples collected before 2019,
192 prior to the emergence of SARS-CoV-2. Compared to pre-COVID samples, the exposed-
193 negative group exhibited significantly higher levels of Spike-specific IgG. These findings
194 suggest that the exposed-negative group may have developed some degree of antigen-
195 specific immunity. This observation is consistent with prior report showing that
196 individuals exposed to a virus do not necessarily develop viremia detectable by PCR, as
197 observed among frontline healthcare professionals during the COVID-19 pandemic (20).
198 Convalescent patients, sampled 20 to 180 days after symptom onset, exhibited higher IgG
199 titers than the exposed-negative group (**Figure 1A**).

200 The presence of anti-Spike antibodies in exposed-negative group prompted us to
201 investigate whether our assay would be sensitive enough to detect relatively rare anti-S
202 specific B cells within the MBC repertoire of SARS-CoV-2 in these individuals. To assess
203 the frequency of Ig-secreting cells, we sorted total switched memory B cells (swMBCs)
204 from both SARS-CoV-2 exposed-negative individuals and convalescent patients and
205 cultured them under LDA conditions. The gating strategy used to isolate total swMBCs
206 (CD19+CD27+CD38-IgD-) is shown in **Figure 1B**. For these initial experiments, we did
207 not use the antigen-baited sorting strategy to enrich for S-specific MBCs as depicted in
208 **Figure 1C**. Instead, total swMBCs were used to explore the unbiased repertoire. The
209 percentage of Ig-secreting cells ranged from 14% to 60%, with no significant differences
210 between negative and convalescent individuals (**Figure 1D**). Quantifying the number of
211 Ig-secreting B cell clones per culture ensures accurate determination of the frequency of
212 antigen-reactive B cells in each sample (8). To maintain an unbiased assessment of
213 antigen-specific responses, we adjusted cell plating densities to calculate the percentage of
214 B cells secreting Spike-specific antibodies. Exposed-negative individuals showed lower
215 S-specific MBC frequencies (0.2%), compared to convalescent patients (1.6%) (**Figure**
216 **1E**). Interestingly, the frequency of IgG+ Spike-specific MBCs correlated with serum IgG
217 anti-S levels in most convalescent donors (**Figure 1F**). These findings demonstrate that
218 our culture method has sufficient sensitivity to identify anti-S B cell clones both in
219 convalescent donors and exposed-negative individuals. LDA further revealed a ~10-fold
220 enrichment of anti-S clones in convalescent donors relative to exposed-negative
221 individuals.

222 While LDA cultures can efficiently quantify antigen-specific MBCs frequencies, these
223 cells represent only a small fraction of the overall MBC repertoire. Moreover, bulk culture
224 LDA systems preclude mRNA isolation from individual B cell clones, impeding
225 downstream transcriptional analysis of the antigen-specific VH/VL repertoire. To address
226 this, we implemented single-cell cultures (SCCs) of antigen-baited sorted MBCs. In these
227 experiments, S-baited MBCs were sorted using Wuhan strain Spike protein labeled with
228 two different fluorochromes, APC and FITC, to ensure cell specificity to the antigen
229 (**Figure 1C**). Spike-baited sorted cells from one patient (5102) were cultured individually
230 with NB21 feeder cells and stimulated with R848 + IL-2. After 7 days, supernatants were
231 analyzed for total Ig secretion and Spike-specific Ig by ELISA. The proportion of Ig-

232 secreting cells in SCCs matched those observed in LDAs (**Figure 1G and H**), confirming
233 that SCCs reliably support single B cell growth and differentiation. Of note, antigen-
234 baiting strategy led to over 30-fold enrichment of Spike-specific cells, increasing their
235 frequency from an average of 1.6% in LDA to ~50% in SCC (**Figure 1G and H**). These
236 results demonstrate that antigen-baited sorted MBCs can grow and differentiate under
237 SCC conditions, facilitating the isolation of Spike-specific monoclonal antibodies and
238 enabling downstream transcriptional analysis of VH/VL repertoires of individual antigen-
239 specific clones.

240 **Single-cell cultures (SCCs) for antigen-directed Ig repertoire analysis and**
241 **monoclonal antibody isolation**

242 Our SCC system enables easy access to monoclonal antibodies in the culture supernatants
243 of bait-selected MBCs for antigen-specific screening. To explore this capability, we
244 analyzed a cohort of eight blood donors with a history of multiple SARS-CoV-2
245 vaccination and/or infection who exhibited high levels of serum-specific antibodies
246 (**Supplementary Figure 2**). Samples were collected in 2022 and 2023, when the
247 Omicron variant was the predominant strain. Spike-specific MBCs were sorted using a
248 bait strategy and subjected to our SCC protocol. After 5 to 7 days of culture,
249 approximately 250 µL of supernatant containing monoclonal Ig was obtained from each
250 SCC well, providing sufficient volume to test each growing clone for total Ig secretion and
251 multiple specificities of the secreted mAb by ELISA. For each individual donor, the total
252 Ig secreted by individual MBC clones in the SCC are displayed in **Figure 2A**, with the
253 frequency of responding B cells ranging from 22% to 54%. An average cloning efficiency
254 of 37% across donors was observed, as measured by total Ig secretion (**Figure 2B**).
255 Among the 592 mAbs produced by responding MBCs, 312 exhibited IgG reactivity
256 against the Wuhan strain Spike protein. Spike-specific clones varied among donors,
257 accounted for 29% to 71% of the Ig-positive wells (**Figure 2C and Supplementary**
258 **Table 1**). On average, 51% of the clones were identified as S-positive (**Figure 2D**),
259 consistent with our findings from the SCC in **Figure 1H**. Importantly, SCCs secreted on
260 average ~142 ng/mL of functional Spike-specific IgG, as defined by calibration against a
261 reference anti-Spike IgG human monoclonal antibody (**Supplementary Figure 2C**).

262 The trimeric SARS-CoV-2 Spike protein consists of three identical subunits, each with
263 distinct functional domains, including the S1 and S2 subunits, as depicted in **Figure 2E**.
264 The S1 subunit contains the receptor-binding domain (RBD), and the N-terminal domain
265 (NTD), while the S2 subunit facilitates the fusion of the virus with the host cell
266 membrane. The RBD is critical for viral entry, as it directly interacts with the ACE2
267 receptor of human cells, making RBD-specific antibodies highly neutralizing due to their
268 ability to block this interaction. NTD-binding antibodies destabilize the Spike protein
269 trimer, impairing its function and reducing infectivity (21, 22).

270 To further characterize the obtained mAbs, we analyzed their binding capacity to the
271 RBD and NTD regions by ELISA. Donors exhibited higher serum IgG levels against RBD
272 than NTD (**Supplementary Figure 2D**). Consistently, RBD-specific clones accounted for
273 33% of cellular responses, compared to 14% NTD-specific clones, aligning with results
274 from previous studies (23). Notably, 53% of clones bound to unknown regions,
275 outnumbered those targeting RBD or NTD (**Figure 2F and G**). We observed a bimodal
276 distribution in the percentage of RBD-specific clones across different donors (**Figure 2G**).
277 For example, donors vaccinated with CoronaVac (CV; donors 1–3) displayed clones that

were negative for both RBD and NTD specificity and had higher frequencies of clones recognizing other regions of the Spike antigen, (**Figure 2F**). Donor 4, also vaccinated with CV, had a history of multiple infections with Wuhan and Omicron variants and exhibited broader responses. In contrast, donors vaccinated with AstraZeneca (AZ; donors 5–7), exhibited a higher frequency of RBD-specific clones. Donor 8, also vaccinated with AZ, displayed a higher proportion of clones binding to other regions (**Figure 2F**). When grouped by vaccine type, distinct patterns of clone specificity emerged. Donors primed with CV exhibited significantly fewer RBD-specific clones compared to those primed with AZ, resulting in a higher frequency of clones recognizing other regions of the Spike antigen (**Supplementary Figure 2E**). The observed frequencies of domain-specific clones align with previous reports on SARS-CoV-2-infected cohorts (24), suggesting that the data obtained with SCC method described here accurately represents the underlying antibody repertoire without introducing artifactual biases.

Comparative cross-reactivity of SCC-derived mAbs to SARS-CoV-2 variants

During the COVID-19 pandemic, identifying mAbs capable of targeting evolutionarily conserved epitopes in the SARS-CoV-2 Spike protein became a major focus due to the virus's high mutation rate. To evaluate this aspect in our system, we conducted a cross-reactivity study using mAbs derived from SCCs obtained from donors with varying anti-Spike serum IgG levels from different variants (**Figure 3A**). We tested the reactivity of these mAbs against the Spike proteins of four major variants of concern (VOCs): Beta ("B"), Delta ("D"), Gamma ("G"), and Omicron BA.2 ("O"). Across the VOCs, the mAbs exhibited a similar average frequency of immunoreactivity, ranging from 46% to 54%, except for Omicron, which showed a lower average of ~30%. The mean immunoreactivity frequencies of mAbs for each variant, stratified by donor, are illustrated in **Figure 3B**. While these data provide an overview of variant recognition by mAbs, they do not differentiate between strain-specific and cross-reactive responses.

To further dissect cross-reactivity, we analyzed 592 mAbs isolated from eight donors. Among these, 217 clones showed no binding to any Spike protein variant (R0), and 312 clones were reactive to the Wuhan strain, with 15 clones binding exclusively this strain. A total of 375 clones were categorized into five reactivity groups based on their binding profiles, encompassing 31 distinct and overlapping categories. The R1 group included clones reactive to a single strain, while R2, R3, and R4 groups represented mAbs binding to combinations of two, three, and four strains, respectively. The R5 group comprised mAbs that were reactive to all five tested strains. These reactivity groups are detailed in **Figure 3C and Supplementary Table 1**, with each group assigned labels reflecting the recognized VOCs, for example "WBO" designates clones that bind the Wuhan, Beta, and Omicron variants.

We analyzed the distribution of these categories among donors, with particular emphasis on domain-specific binding among R5 clones, which exhibited the highest degree of cross-reactivity across all tested VOCs (**Figure 3D**). Within the R1 group, we found 15 clones binding exclusively to Wuhan, and 12, 11, 10 and 8 mAbs binding to Gamma, Delta, Omicron, and Beta, respectively. The R1 group, representing strain-specific antibodies, is useful for highly specific immunological assays. R2 and R3 mAbs, which bind two or three strains, are valuable in immunocompetition assays probing inter-variant interactions. R4 antibodies, reactive to all but one variant, help identify signatures of broad binding and structural or genetic factors that impair recognition of particular

VOCs, such as Omicron. Comparing R4 and R5 mAbs could reveal key molecular features underlying broad reactivity. Antibodies in the R5 group, which recognize all five variants, likely target highly conserved epitopes, making them particularly valuable for therapeutic applications.

While a distinct distribution of cross-reactive clones was observed across donors (**Figure 3D**), most clones fell into R4 and R5 groups, with 111 R4 clones, 95 of which were specifically classified as R4 (WDBG), and 152 R5 clones (**Supplementary Table 1**). We performed a comparative analysis of mAbs within these two categories, particularly the R4 (WDBG) group, recognizing all variants except Omicron, and the R5 group, which includes antibodies reactive to all five tested strains (**Figure 3E**). Broadly cross-reactive clones are generally expected to target conserved regions of the Spike protein, such as the S2 region, making RBD and NTD less likely targets. This pattern held for R4 (WDBG) antibodies, with 82% of clones binding to the putative S2 region, or other undefined domains (non-RBD/NTD). Surprisingly, 54% of the R5 mAbs bound either RBD (35%), NTD (15%), or both (4%), suggesting that a substantial fraction of these antibodies may possess substantial broadly neutralizing potential.

The cross-reactivity analysis effectively dissects the frequency of strain-specific and cross-reactive mAbs but did not provide insights into the strength or affinity of antibody binding. To address this limitation, we employed a heatmap representation as an alternative approach to visualize the complexity of cross-reactive analysis, providing at least a semi-quantitative assessment of the relative binding strength of each mAb. Binding intensity was evaluated using the ELISA optical density (O.D) ratio, calculated as the antigen-specific O.D. divided by the assay cut-off (defined as the average background signal plus three standard deviations). An O.D. ratio above 1 was considered positive. **Supplementary Figure 3** illustrates the binding intensity of each R5 mAb isolated to the Spike protein of the tested VOCs, including key neutralizing antibody targets such as the RBD and NTD. Clones were ordered in descending binding intensity to the Wuhan strain and labeled sequentially from R5-001 to R5-152 (**Supplementary Figure 3A)**. They were also ranked based on Omicron binding intensity (**Supplementary Figure 3B**). Notably, mAbs exhibiting higher binding intensity for Wuhan Spike were predominantly RBD-specific. This visualization facilitated the identification of clusters of clones with similar binding intensity, enabling the selection of specific candidates tailored to particular study designs. For instance, in the heatmap, we highlight clones chosen for downstream functional analysis, demonstrating the utility of this approach in prioritizing mAbs for further investigation.

SCC supernatants support neutralization assays and functional mAb candidate selection

To functionally characterize the broadly binding R5 antibodies, we selected three SCC-derived mAbs for pseudovirus neutralization assay against the Omicron variants BA.1 and BA.2: two RBD-binding mAbs (R5-004 and R5-038) and one mAb that does not appear to bind either RBD or NTD (R5-053). The Omicron strain was chosen due to its generally lower intensity of binding observed in prior assays and its high divergence compared to the original Wuhan strain. As shown in **Figure 3F** these mAbs exhibited variable neutralization capacity against the BA.1 variant. The RBD-binding mAb R5-004 demonstrated strong neutralization potential, achieving half-maximal inhibitory concentration (IC50) values in the range of 0.001–0.01 μg/mL. In contrast, RBD-binding

370 mAb R5-038 and the non-RBD/NTD binding clone R5-053 showed moderate to weak
371 neutralizing activity, with IC50 values ranging from 0.01–0.1 μg/mL for the first and a
372 limit of 50% neutralization at the highest concentration used (> 0.1 μg/mL), respectively.
373 Notably, none of the tested mAbs were able to neutralize the BA.2 variant (data not
374 shown), underscoring the increased challenge posed by this more divergent Omicron
375 subvariant. The systematic evaluation of SCC-derived mAbs demonstrates the utility of
376 our platform in mapping cross-reactive and strain-specific antibody responses. These
377 findings lay the groundwork for developing diagnostic and therapeutic tools targeting
378 SARS-CoV-2 and its evolving variants.

379 **SCC method enables immunoglobulin repertoire analysis and reveals convergent V**
380 **region rearrangements**

381 Our SCC platform allows to interrogate the clonotypic immunoglobulin repertoire at the
382 transcriptional level. mRNA from expanded SCC-derived MBCs was extracted and
383 subjected to *Ig* heavy and light chain sequencing using V region-specific RT-PCR
384 followed by Sanger sequencing. We sequenced a total of 240 of Ig-secreting MBCs, of
385 which 220 were identified as IgG+ Spike-specific clones. To validate that our culture
386 system did not distort the B cell repertoire, we analyzed the V_H gene segment usage and
387 compared the frequencies to a dataset of healthy individuals, and with previous COVID-
388 19 studies (**Figure 4A**). Our findings revealed that gene segments IGHV3-30, IGHV5-51,
389 IGHV3-66, and IGHV1-24 were significantly overrepresented in our cohort, whereas
390 IGHV1-18, IGHV3-23, and IGHV1-69 were underrepresented (**Figure 4A**). Notably, the
391 high frequency of IGHV3-30 aligns with its consistent identification in SARS-CoV-2
392 antibody repertoire studies (14, 25-28).

393 Throughout the COVID-19 pandemic, significant efforts were made to identify
394 common features of protective antibody responses against SARS-CoV-2 (26, 29, 30). A
395 seminal study highlighted specific patterns in the immunoglobulin V region, such as V
396 gene usage bias and CDR-H3 composition, associated with binding to RBD, NTD, or S2
397 regions (27). Here, we compared our data to these previously described patterns to identify
398 convergent antibody responses. Each SCC-derived clone had their mAb-enriched
399 supernatants tested for binding to the full Spike protein and to isolated RBD and NTD
400 domains. This enabled classification of clones into three groups: RBD+ (S1), NTD+ (S1),
401 and non-RBD/NTD (putative S2- or other-region binders). Among 220 S-binding clones,
402 25% were RBD+, 13% were NTD+, and 62% were RBD-/NTD- (**Figure 4B**).

403 Efforts to identify potent neutralizing antibodies against SARS-CoV-2 have
404 highlighted the importance of paralogous genes IGHV3-66/V3-53, which are enriched in
405 RBD-binding clones (31-36). In our data, IGHV3-66 was five times more frequent
406 compared to the healthy repertoire (**Figure 4A**). Although only 25% of total clones were
407 RBD+ (**Figure 4B**), 71% of IGHV3-66 clones were RBD+ (**Figure 4C and 4D**).
408 Conversely, a strong bias toward IGHV3-30 usage has been observed in S2-binding
409 antibodies (27). Consistent with this, most IGHV3-30 clones in our study were classified
410 as RBD-/NTD- (**Figure 4C, 4D**). Light chain V gene usage also exhibited domain-related
411 biases. For instance, IGKV3-20 was associated with S2-targeting antibodies, while
412 IGKV1-9 and IGKV1-33 were prevalent among RBD-binding clones (**Supplementary**
413 **Figure 4A and 5A**) (34).

414 Since our mAbs were tested for RBD and NTD binding via ELISA but not for S2
415 binding, we cannot experimentally confirm here that the RBD-/NTD- clones specifically
416 target this region. To address this limitation, we performed *in silico* docking studies to
417 assess our presumption. First, we validated the docking approach by submitting two RBD-
418 binding clones for analysis, which confirmed their preferential binding to the RBD region
419 of the Spike protein (**Supplementary Figure 4A**). To investigate whether the putative S2-
420 binding clones indeed targeted the S2 region, we selected four RBD-/NTD- clones for
421 docking analysis, including two encoded by the IGHV3-30 gene segment (22E1P2E08
422 and 22E1P1B05). The docking results supported their binding preferences for regions
423 within the S2 domain (**Supplementary Figure 4B**), providing further evidence for their
424 classification as S2-binding clones.

425 We next investigated whether our dataset contained convergent paired IgH/IgL
426 antibody sequences matching those reported in other SARS-CoV-2 studies. Convergent
427 sequences were defined as those sharing the same VH/JH and VL/JL gene usage (allowing
428 minor exceptions for light chains) and exhibiting at least 80% CDRH3 sequence identity.
429 Despite the substantial combinatorial and junctional diversity of the human antibody
430 repertoire, we identified at least 10 clones from our dataset that matched sequences
431 previously reported in independent SARS-CoV-2 studies (14, 27, 31, 37-42). Our analysis
432 revealed four RBD-specific sequences and six putative S2-specific sequences highly
433 similar to clones described in prior datasets (**Figure 4E**), providing further validation of
434 our methodology and supporting the conserved nature of these antibody responses.

435 The distribution of CDR-H3 amino acid length of mAbs reflected a typical human
436 repertoire (43). Clones classified as RBD^{-}/NTD^{-} (putative S2-binding) most frequently
437 exhibited CDR-H3 loops of 14 amino acids, whereas 11 amino acids predominated in
438 RBD^{+}/NTD^{+} clones (**Supplementary Figure 5B and C**). This pattern aligns with findings
439 from Wang et al., where three major S2-binding clusters had CDR-H3 lengths of 14 amino
440 acids (27). Interestingly, the mean CDR-H3 length for NTD-binding clones was longer
441 averaging 18 amino acids compared to 15 for RBD and RBD-/NTD- clones
442 (**Supplementary Figure 5C**).

443 Charge distribution within the CDR-H3 loop was similar across groups, with a
444 tendency toward neutrality (**Supplementary Figure 5D and E**). No overall differences in
445 amino acid composition were observed between the RBD-/NTD- (S2) and RBD+/NTD+
446 (S1) groups (**Supplementary Figure 4F**). To delve deeper into potential domain-specific
447 differences, we analyzed clones with biased CDR-H3 lengths, 14 amino acids for the
448 RBD-/NTD- group and 11 amino acids for the RBD+ group, focusing on their amino acid
449 content. Significant differences were observed: RBD-/NTD- (S2) clones with 14 amino
450 acid CDR-H3 loops showed increased use of neutral amino acids such as Tyr, Gly, and
451 Ser, compared to RBD+ clones (**Supplementary Figure 5G and data not shown**). A
452 conserved motif 97[S/G]G[S/N]Y100 was identified in RBD-/NTD- clones such as
453 22E1P1B05 (**Figure 4E and Supplementary Figure 4B**), consistent with previous
454 studies (27). In contrast, clones with 11-residue CDR-H3 loops showed no clear bias for
455 neutral amino acids in either S1 or S2-targeting groups (**Supplementary Figure 5G**).

456 The level of somatic hypermutations (SHM) did not seem to differ among clones that
457 target the different domains (**Figure 4F**). The 240 clones were also analyzed for antigenic
458 breadth and classified based on their ability to recognize S protein variants using the
459 cross-reactivity scale, R0-R5 (**Figure 4G**). Importantly, the largest group was R5 (41.7%)

460 followed by R4 (32.5%). The main distinction between R5 and R4 is the ability to
461 recognize Omicron Spike, the most divergent variant tested. Clones recognizing the 5
462 VOCs, including Omicron (R5), appeared to accumulate more point mutations than those
463 that could not bind Omicron (**Figure 4H**), suggesting a role for SMH and affinity
464 maturation in broadening antibody reactivity. Altogether, these findings establish the SCC
465 platform as a powerful and reliable tool for comprehensive, antigen-specific
466 immunoglobulin repertoire studies, while also highlighting critical conserved features of
467 SARS-CoV-2 convergent antibody responses.

468 **SCCs enable functional antigen-specific mAb screening, reducing time and resources**
469 **before scale-up**

470 The SCC methodology effectively identifies antigen-specific and cross-reactive mAbs,
471 streamlining the selection process before large-scale production. As VH/VL sequences can
472 be retrieved from single B cell cloning cultures, this approach enables the subsequent
473 production of large quantities of selected recombinant mAbs for downstream applications,
474 including functional assays, structural studies, and therapeutic development. At the onset
475 of the COVID-19 pandemic, before vaccines were available in Brazil and before the
476 global spread of variants, we isolated several mAbs from patients who recovered from the
477 original Wuhan strain (Cohort 1, **Figure 1**). From this cohort, we selected two broadly
478 reactive RBD-binding clones identified in our 2020 screening assay to evaluate their
479 cross-reactivity and neutralization potential. The Ig genes from these clones were
480 sequenced and expressed in Expi293 cells. Interestingly, these clones expressed
481 convergent V-region rearrangements, including public V3-53 and V3-66 antibodies,
482 consistent with findings that were later published by several groups, (26-28, 31, 36, 37,
483 44). The selected clones were encoded by VH3-53 (LBL01) and VH3-66 (LBL02), both
484 using VK1-9 for their light chains. The CDR-H3 and CDR-L3 sequences, along with V
485 and J segment usages, are shown in **Figure 5A**.

486 Computational docking analysis corroborated the binding of both clones to the RBD *in*
487 *silico* (**Figure 5B**). Further blind docking analyses against multiple VOCs revealed limited
488 cross-reactivity for LBL01, whereas LBL02 exhibited the potential to a broader reactivity
489 as distinct docking runs converging on a similar binding site (**Supplementary Figure 6**).
490 Accordingly, molecular dynamics simulations of the refined interaction poses followed by
491 binding free energy ($\mathbf{\Delta G_{bind}}$) calculations, revealed a stronger interaction of LBL02 with
492 the RBD (-49.4 kcal/mol) compared to LBL01 (-42.3 kcal/mol), suggesting a more stable
493 binding interface that may confer greater resistance to viral escape (**Figure 5B**;
494 **Supplementary Figure 6)**.

495 The two mAbs were then produced at scale from Expi293 cultures, purified, and
496 tested for binding to S proteins from Wuhan, Delta, Beta, Gamma, and Omicron (BA.2),
497 as well as to the isolated RBD and NTD domains (**Figure 5D**). Both antibodies were
498 confirmed to target the RBD. Titration experiments demonstrated that LBL01 exhibited
499 relatively weak binding to VOCs S proteins compared to LBL02, which displayed strong
500 apparent affinity across all tested variants. Pseudovirus neutralization assays were
501 performed against Wuhan and VOCs, including Delta, Beta, Gamma, and Omicron (BA.2,
502 BA.1, and XBB). Consistent with binding and *in silico* analyses, LBL01 showed weaker
503 neutralization against Delta, BA.1, and Wuhan strains but retained limited activity against
504 the Omicron subvariants BQ.1 and XBB. In contrast, LBL02 strongly neutralized Wuhan
505 and Delta but showed sharply reduced activity against Omicron subvariants (**Figure 5E**).

506 These findings suggest that some early-pandemic immune responses may have conferred
507 cross-protection against emerging variants, emphasizing the importance of rapidly
508 identifying broadly neutralizing antibodies for future pandemic preparedness.

509 Altogether, these findings demonstrate that the SCC platform enables efficient
510 selection of clones with desired specificity and functional neutralizing potential prior to
511 scaling up production. This method reduces the time and resources typically required for
512 traditional cloning and expression workflows, providing a streamlined and cost-effective
513 approach for monoclonal antibody discovery.

514 **Discussion**

515 Memory B cells are essential components of the adaptive immunity, enabling rapid and
516 robust responses upon re-exposure to pathogens. While serum antibody titers provide a
517 snapshot of circulating immunity, MBCs represent the capacity for secondary responses
518 upon antigen re-exposure, providing a dynamic perspective on immune memory. By
519 isolating and characterizing these cells, researchers can explore the mechanisms
520 underlying long-term immunity, yielding valuable insights for vaccine and
521 immunotherapy development. Such studies are particularly critical for emerging infectious
522 diseases, where timely and precise immune responses can be pivotal in controlling
523 outbreaks. MBC-derived mAbs have revolutionized treatment strategies for diseases like
524 COVID-19. These studies not only deepen our understanding of immunity but also
525 provide practical tools for combating infectious and autoimmune diseases (37, 45, 46).

526 We previously developed a method for studying the mouse B cell repertoire,
527 combining high-efficiency B cell cultures supported by feeder cells with single-cell RT-
528 PCR amplification of Ig variable genes and sequencing (10). This approach provides
529 access to the entire naïve and memory B cell repertoire, simultaneously enabling antigen
530 specific analysis and VH/VL repertoire usage. Here, we adapted this strategy to analyze
531 the human MBC repertoire and established a streamlined pipeline for isolating specific
532 human monoclonal antibodies. Our goal was to democratize access to comprehensive
533 humoral immune profiling, enabling a wide range of laboratories to address local
534 infectious disease challenges with innovative solutions to support both immunological and
535 translational studies.

536 It is noteworthy that all the feeder cells used in our study were derived from mice, yet
537 they effectively support the growth and differentiation of human B cells in culture. This
538 cross-species compatibility suggests that key survival and activation signals provided by
539 these feeder cells may be shared across species. Among the tested feeder cell lines, NB21
540 cells, engineered to secrete IL-21, were the most effective in supporting MBC survival and
541 promoting immunoglobulin secretion. IL-21 boosts immunoglobulin production,
542 particularly IgG, which is crucial for functional antibody repertoire analyses. While the
543 prevailing protocols for culturing human MBCs with feeder cells rely on complex
544 cytokine cocktails (12, 13), our culture system employs a simplified yet effective strategy
545 inspired by Pinna et al. (2009) (8). These authors optimized human MBC proliferation and
546 Ig secretion using R848 or CpG combined with high-dose IL-2 (8). Given R848's cost-
547 effectiveness and dual activation of TLR7 and TLR8, here we chose R848 as a polyclonal
548 stimulus in our culture system. Therefore, by combining NB21 cells, R848 polyclonal
549 stimulation, and IL-2 supplementation, we successfully establish here a robust and
550 reproducible platform for both quantifying the frequency of antigen-specific human MBCs
551 clones and characterizing their VDJ/VJ repertoire.

552 Our data show that the methodology is sensitive enough to detect and characterize
553 antigen-specific MBC responses in both SARS-CoV-2-exposed donors and convalescent
554 patients. The results underscore the sensitivity and reliability of the proposed platform for
555 studying and comparing MBCs responses across individuals and experimental groups
556 using a standardized feeder cell system, thereby assuring reproducibility. The ability to
557 capture low-frequency antigen-specific MBCs is relevant for understanding immune
558 memory, given the vast antigenic repertoire that MBCs must encode over a lifetime.
559 Traditional approaches often struggle to reveal these rare populations due to their low
560 abundance. Here we show that the antigen-specific repertoire can be probed using LDA

561 cultures. Our methodology demonstrated sufficient sensitivity to distinguish SARS-CoV-
562 2-exposed donors from convalescent patients sampled in 2020. Interestingly, we observed
563 a correlation between Spike-specific MBC frequencies and serum anti-Spike IgG levels.
564 Similar correlations have been reported in previous studies of patients exposed to antigens
565 through immunization or infection (5). This correlation supports the use of MBC profiling
566 as a complementary tool for immunoepidemiological surveillance of pathogen exposure
567 and immune memory.

568 To facilitate the isolation of antigen-specific MBCs for mAb production, we employed
569 a baiting strategy using Wuhan strain Spike protein conjugated to two different fluorescent
570 markers (**Figure 1 C**). We showed that SCCs of bait-sorted cells yielded total percentages
571 of responding B cells comparable to those obtained through LDA of total MBCs, while
572 significantly enhancing the isolation of antigen-specific mAbs. These results demonstrate
573 that bait-selected B cells maintain viability and are not prone to cell death potentially
574 induced by B-cell receptor cross-linking. Notably, the baiting strategy increased the yield
575 of antigen-specific mAbs by 30- to 50-fold compared to cultures of MBCs isolated
576 without antigen baiting.

577 A key aspect of our SCC platform is the ability to rapidly generate monoclonal
578 antibodies to interrogate multiple specificities within a single antibody sample. Despite the
579 limited supernatant volume recovered from SCCs, we demonstrated the feasibility of
580 performing pseudovirus neutralization and multiple ELISA assays to identify antigen-
581 specific responses and prioritize the most promising mAbs to sequencing. This is
582 particularly beneficial in scenarios where logistical or financial constraints prevent the
583 sequencing of a large number of mAbs. Compared to traditional hybridoma and
584 recombinant mAbs techniques, SCCs offer a crucial advantage by streamlining the
585 identification of antigen-specific clones, eliminating labor-intensive and financially
586 expensive steps such as massive gene sequencing and recombinant mAb expression.
587 These findings highlight the utility of our SCC-based approach as a time-efficient and
588 cost-effective solution for both antibody repertoire analysis and monoclonal antibody
589 discovery.

590 The Spike protein is the most immunodominant antigen of SARS-CoV-2. Most
591 antibodies targeting Spike recognize the S1 subunit with anti-RBD antibodies accounting
592 for nearly 90% of the neutralizing antibodies found in convalescent plasma from COVID-
593 19 patients (47). The RBD is well established as a critical target for neutralizing antibodies
594 due to its role in binding ACE2 receptor, a key step in viral entry (48). However, the NTD
595 of the S1 subunit also contains an antigenic "supersite" that serves as a major target for
596 antibody responses (49). Notably, as SARS-CoV-2 has evolved, the S1-NTD has
597 accumulated numerous mutations, particularly deletions, which can alter antigenicity or
598 eliminate key epitopes. These alterations enhance the virus's ability to evade immune
599 recognition, further complicating the maintenance of effective immunity through
600 vaccination or natural infection (50-53). The RBD, especially in variants of concern
601 (VOCs) such as Delta and Omicron, is under intense mutational pressure, posing a
602 significant challenge for vaccine-induced and natural immunity. Antibodies binding to
603 evolutionary conserved epitope within RBD that can recognize all VOCs hold great
604 potential for cross-protective immunity. Similarly, the NTD plays a multifaceted role in
605 viral attachment and entry, but is also prone to mutations and deletions that alter
606 antigenicity and enable immune evasion (53). These structural changes in both RBD and

607 NTD contribute to the virus's ability to escape recognition, complicating vaccine efficacy
608 and the design of therapeutic antibodies.

609 In the present work, we isolated 592 mAbs, 312 of which recognized the Wuhan strain
610 Spike protein. Given the well-known immunodominance of the RBD and NTD of the
611 Spike protein (47, 48, 53), we classified mAb specificities within our collection
612 accordingly. Interestingly, the majority of isolated mAbs in this study were non-RBD/non-
613 NTD specific, suggesting that these antibodies may target other S1 conformational
614 epitopes or conserved regions on the S2 subunit, areas not directly tested in our assay. The
615 S2 region, which mediates viral fusion, is less prone to mutations than S1, making it an
616 attractive target for broad-spectrum neutralizing antibodies. The high proportion of non-
617 RBD/non-NTD antibodies observed in our study, is consistent with the predominance of
618 non-RBD/non-NTD antibodies reported in the literature (24). These findings emphasize
619 the importance of expanding the scope of epitope targeting to include non-RBD/non-NTD
620 conserved regions for the development of universal vaccines and therapeutics against
621 SARS-CoV-2 and its variants.

622 The NTD of the SARS-CoV-2 Spike protein is susceptible to frequent mutations and
623 deletions. These structural changes, commonly observed in several VOCs including Delta
624 and Omicron, significantly contribute to immune escape, thereby impacting vaccine
625 efficacy and natural immunity. Here, we utilized the NTD protein from the Wuhan strain
626 in the ELISA assays. As expected, our analysis revealed that, on average, the NTD region
627 was less frequently recognized by the isolated monoclonal antibodies compared to the
628 RBD and other unidentified regions, in agreement with previous studies. Interestingly, a
629 bimodal distribution of RBD-specific clone percentages among donors became evident
630 when grouped by vaccine type. Most CoronaVac (CV) vaccine recipients displayed a
631 higher proportion of clones recognizing non-RBD/non-NTD regions, whereas 3 out of 4
632 AstraZeneca (AZ) vaccine recipients exhibited a greater frequency of RBD-specific
633 clones. This variation likely reflects differences in vaccination regimens, prior exposure to
634 diverse viral variants, or underlying genetic heterogeneity among donors.

635 The cross-reactivity analysis performed here, across Spike proteins, revealed distinct
636 patterns of strain-specific and broadly reactive antibodies, offering valuable insights into
637 the immunological landscape of SARS-CoV-2 and its variants (50-53). Notably, we
638 successfully identified several R5 mAbs that bind to all tested variants. Throughout the
639 COVID-19 pandemic, a key priority has been the identification of mAbs that can target
640 conserved regions of the SARS-CoV-2 Spike protein due to their therapeutic potential. R5
641 antibodies, which recognize all tested variants, likely target highly conserved epitopes,
642 making them particularly promising candidates for broad-spectrum antiviral strategies.
643 These conserved binding sites suggest a greater potential for neutralization breadth, a
644 critical attribute given virus's high mutational rate and the emergence of variants with
645 enhanced transmissibility or immune escape. Antibodies targeting such sites could be
646 instrumental for developing treatments and vaccines that are effective across multiple
647 strains, enhancing the prospects for broader and more durable immunity, offering a critical
648 advantage in controlling outbreaks and mitigating the risk posed by future variants.
649 Comparative analyses between R4 and R5 clones may further illuminate the molecular
650 determinants of broad reactivity, contributing to the design of next-generation
651 immunotherapies. In parallel, strain-specific antibodies, such as those in the R1 group,
652 also hold significant value as precise tools for detecting individual variants, making them
653 useful for variant-specific diagnostic assays.

654 Broadly reactive clones were isolated in the present study through SCC supernatant
655 screening, including R5-004 and R5-053. As a proof of concept to demonstrate the
656 method's capability to use supernatants containing mAbs to identify clones with potential
657 for virus neutralization, we cloned and expressed two public RBD-specificantibodies,
658 LBL01 and LBL02. Functional assays performed with the recombinant antibodies were in
659 full agreement with those obtained with their respective SCC-derived supernatants. These
660 results validate the platform's utility for the characterization and isolation of antibodies
661 with therapeutic and diagnostic applications.

662 The high cloning efficiency of our SCC system with NB21 feeder cells enabled
663 unbiased profiling of memory B cells (MBCs) repertoire, revealing convergent
664 rearrangements in immunoglobulin variable (V) regions that align with findings from
665 previous SARS-CoV-2 studies (26, 27, 54). Key aspects include the representation of VH
666 gene segments, particularly IGHV3-30 and IGHV3-53/IGHV3-66, and their association
667 with distinct Spike regions. Importantly, VH/VL analysis of SCC-derived clones exhibited
668 somatic hypermutations correlating with cross-reactivity, particularly for challenging
669 variants like Omicron. Consistent with earlier studies, IGHV3-53/IGHV3-66 was strongly
670 linked to RBD-binding antibodies, while IGHV3-30 was primarily associated with
671 putative S2-targeting clones (27). Computational docking confirmed these classifications,
672 providing evidence for conserved binding motifs and structural preferences. The
673 paralogous genes IGHV3-53 and IGHV3-66 are frequently described as encoding public
674 clones across diverse populations (36, 55). Interestingly, while most global studies report a
675 higher prevalence of IGHV3-53 compared to IGHV3-66, our dataset showed a fourfold
676 higher frequency of IGHV3-66 among RBD-binding antibodies. This distinctive finding
677 might reflect a population-specific features of the Brazilian cohort, as a similar preference
678 for IGHV3-66 was observed in another study involving Brazilian blood donors (25).

679 Limitations of this study include the use of Wuhan strain-based reagents, which may
680 underestimate responses to more recent variants. Additionally, the classification of mAbs
681 as non-RBD/non-NTD was based on lack of reactivity rather than confirmed S2 binding,
682 underscoring the need for further site-specific targeting. While *in silico* analyses support
683 these assignments, structural validation would strengthen the conclusions. The SCC
684 methodology, although effective for identifying antigen-specific and cross-reactive mAbs,
685 yields limited antibody quantities, sufficient only for initial screening. However, because
686 VH/VL sequences can be retrieved from SCCs, this limitation can be addressed through
687 recombinant expression of selected clones. Finally, the small number of patients studied
688 here limits our ability to draw conclusions about the clonal distribution of memory B cell
689 repertoires and their persistence following vaccination. With expanded cohorts, however,
690 this approach may prove valuable as a novel tool for immunoepidemiological surveillance.

691 In summary, this study presents a reliable methodology for isolating clinically relevant
692 monoclonal antibodies. By enabling functional screening of antigen-specific mAbs
693 directly from culture supernatants, our SCC platform provides insights into binding
694 properties, site specificity, cross-reactivity, and neutralization potential. It simplifies mAb
695 discovery by reducing the need for large-scale sequencing and early recombinant antibody
696 production, thereby lowering costs and labor. This strategy improves workflow efficiency
697 by prioritizing clones for downstream applications based on functional data. Its
698 affordability and adaptability make it valuable for laboratories worldwide, particularly in
699 low- and middle-income regions, by equipping researchers with practical tools for
700 immunological analysis and therapeutic development. Importantly, the platform opens

701 new avenues for immune-epidemiological investigations beyond serology, allowing
702 studies that link the quality and magnitude of memory B cell responses with protection,
703 serum titers, and clonal repertoire composition.

704 **Materials and Methods**

705 **Ethic Statement**

706 This study was approved by the National Ethics Committee (CONEP, Brazil; CAAE:
707 30161620.0.0000.5257) and the local ethics committee of Fundação Oswaldo Cruz
708 (CAAE: 3048.7120.2.0000.0008). Blood collection from the volunteers in this study was
709 carried out at the Diagnostic Center of Núcleo de Enfrentamento e Estudos de Doenças
710 Infecciosas Emergentes e Reemergentes (NEEDIER) located at the Universidade Federal
711 do Rio de Janeiro and at Fundação Oswaldo Cruz, in adherence to the approved protocols

712 **Study Participants**

713 For the first part of the study, involving Limiting Dilution Assay (LDA) culture
714 experiments, we enrolled fourteen patients from Brazil, collecting whole blood samples at
715 NEEDIER to perform Limiting Dilution Assay experiments. For single cell culture
716 experiments for monoclonal antibody isolation, we enrolled eight vaccinated and
717 convalescent patients as described in **Supplementary Figure 2 A**. These patients were
718 selected through Fundação Oswaldo Cruz, with whole blood samples collected for further
719 analysis. Participants were categorized into three cohorts. The first cohort consisted of
720 healthcare workers with consecutive negative PCR results (negative exposure group, n =
721 5). The second cohort included non-vaccinated convalescent individuals, sampled 20 to
722 180 days after their first negative PCR result (n = 9). Samples from these two cohorts were
723 collected in 2020, before COVID-19 vaccines became available. The third cohort
724 comprised individuals with multiple vaccinations and convalescent from prior SARS-
725 CoV-2 infection (n = 8). Additionally, as a control we included 23 pre-COVID plasma
726 samples collected at the State Hematology Institute Hemorio followed a protocol approved
727 by the local ethics committee (CEP Hemorio; approval #4008095).

728 **Blood sample processing**

729 All blood samples were collected in tubes with heparin as an anticoagulant and sent to the
730 Laboratory of Lymphocyte Biology (LBL) for subsequent PBMC isolation. To obtain the
731 desired cell population, we followed the purification protocol using Ficoll Histopaque®-
732 1077 (SIGMA-Aldrich cat.#10771). After allowing the sample to settle for 40 minutes at
733 RT, the tubes containing the sample were centrifuged at 1500 rpm for 5 minutes at 24ºC.
734 Next, the plasma was removed and frozen, and the blood was carefully transferred to a 15
735 mL falcon tube containing 5 mL of Ficoll at a 2:1 dilution. This tube was centrifuged
736 again, this time for 30 minutes at 400g, 24ºC, without brake or acceleration. The PBMC
737 layer was then collected, washed with 1x PBS, and centrifuged at 1300 rpm for 5 minutes
738 at 24ºC. After this step, the pellet was resuspended in 2 mL of ACK Lysing Buffer®
739 (GIBCO, #A10492-01) to lyse red blood cells, keeping the sample in the refrigerator for 5
740 minutes. After a wash step as described previously the cells was resuspended in FACS
741 Buffer containing the labeled antibodies for staining.

742 **ELISA for detection of serum immunoglobulins**

743 For quantitative analysis of anti-SARS-CoV-2 spike protein IgG antibodies, we performed
744 the S-UFRJ test, as described previously (56). Briefly, high binding ELISA plates were
745 coated with 50 µL of SARS-CoV-2 spike protein (4 µg/mL in PBS) and incubated
746 overnight. The coating solution was removed and 100 µL of PBS 1% BSA (blocking

solution) was added and the plate was incubated at room temperature (RT) for 1-2 hours. The blocking solution was removed and 50 µL of diluted 1:40 (PBS 1% BSA) patient sera were added, subsequently, the sera were serially three-fold diluted in the plate, which was incubated at RT for 2 hours. Then, the plate was washed with 150 µL of PBS (5x) and 50 µL of 1:10000 goat anti-human IgG (Fc)-horseradish peroxidase antibody (Sourthen Biotech, Birmingham, USA) were added, and the plate was incubated for 1.5 hours at RT. The plate was washed again with 150 µL of PBS (5x) and then treated with TMB (3,3',5,5-tetramethylbenzidine) (Scienco, Brazil) until the reaction was stopped with 50 µL of HCl 1N. The optical density (OD) was read at 450 nm with 655 nm background compensation in a microplate reader (Bio-Rad Laboratories, Inc, California, USA). Relative antibody levels were determined based on a cut-off (C.O) value calculated as the mean absorbance of the negative controls plus one standard deviation on the same ELISA plate. Samples with absorbance values below the C.O were classified as negative, while those with values at least two times above the C.O were considered positive.

Feeder cell lines preparation

The feeder cells are cultured in T175 flasks (Falcon, Ref #353112) until they reach confluence, using RPMI (Gibco, #11875-093) supplemented with 1% pyruvate (Gibco, #11360-070), 1% glutamine (Gibco, #25030-081), 1% penicillin-streptomycin (Gibco, #15140-122), 1% HEPES (Gibco, #15630-080), 50 nM 2-Mercaptoethanol (Sigma, #M3148), and 10% fetal bovine serum (FBS, Gibco, #10437-028). The cells are passaged every three days. Upon reaching confluence, the cells are detached by treating them with trypsin (Gibco, #15400-054) for 5 minutes at 37°C and 5% CO_2. The culture medium is collected, and the cells are washed with PBS. After centrifugation at 300g for 5 minutes, the pellet is resuspended in 10 ml of RPMI. The cells are then counted using a Neubauer chamber. For plating, 3000 NB21 feeder cells are seeded per well in 100 µl of RPMI with the aforementioned supplements and allowed to grow overnight. The following day, the cells are irradiated with 20 Gy to halt the cell cycle. This irradiation is performed at the Laboratório de Instrumentação Nuclear (LIN), Centro de Tecnologia da UFRJ.

Cell sorting

The cells were stained in supplemented RPMI using CD19 – BV421, CD38 – Pecy5, CD27 – PE, IgD – Pecy7, DUMP(CD3/CD14/CD16) – APCcy7 and Spike-protein labeled with Alexa 488 and Alexa 647 to access the swMBC population ($CD19^{+}CD38^{-}CD27^{+}IgD^{-}$) and antigen-specific swMBC populations ($CD19^{+}CD38^{-}CD27^{+}IgD^{-}Spike^{APC+FITC+}$). Cells were sorted using MoFlo (Dako cytomation) in 5ml tubes with supplemented RPMI.

B cell cloning cultures

Sorted cells were counted and plated using different densities of cell in LDA or 1 cell per well in SCC. In LDA, since the number of B cells were variable among the patients, we plated in the first row 500 to 2000 cells in eleven columns of a 96 well culture plate flat bottom descending in a 3 fold dilution in the first 4 rows of the plate, the for last rows were plated to tending to zero so it can be possible to calculate Poisson distribution.

We plate the 100µl with the determined number of MBC (LDA or SCC) over a monolayer of NB21 cells and supplemented with the polyclonal stimuli of IL-2 (10nM) and R848 (2µg/ml). In this comparison, R848 (Resiquimod) (Invivogen, #tlrl-r848) and IL-2

790 (Immunotools, #11340025) were used as polyclonal stimuli, based on previous reports
791 demonstrating their effectiveness in human B cell cultures (8). The cells were left to grow
792 for 5 days, then we collect 25µl of the supernatant to perform the ELISA for detect total
793 immunoglobulin. In the day 6, we collect another 15µl to perform the antigen-specific
794 ELISA. We stop the culture in day 7, removing and storage the supernatant with 0.02%
795 Azide in another 96 well plate. And the B cells were harvested with 200µl of cold PBS 1x
796 and transferred to a PCR plate with 10 µl of TLC + 5% 2-Mercaptoethano for
797 Immunoglobulin gene sequencing.

798 **ELISA for total immunoglobulins in LDA**

799 High binding ELISA 96-well microplates (Corning) were coated with 50 µL per well
800 using 1:1000 dilution of Ig unlabeled (Southern Biotech #) in PBS 1x for 4°C overnight.
801 In the next day, plates were blocked with 200µl of blocking buffer (PBS 1x with 1% of
802 BSA) for 1h at RT. The blocking buffer was removed, and supernatant was plated diluted
803 two times using blocking buffer in a total volume of 50µl for 2h at RT. The plates were
804 washed five times with 200µl per well of PBS 1x. We used an Ig conjugated with HRP as
805 a secondary antibody using a concentration of 1:4000 dilution in blocking buffer in 50µl
806 per well. The plates were washed as described above and developed with 50 µL of TMB
807 (Scienco, Brazil). The reaction was stopped with 50 µL of 1 N HCl, and the optical
808 density (O.D.) was read at 450 nm with 655 nm background compensation in a microplate
809 reader (BioRad). Positive antibody levels were determined based on a cut-off (C.O) value
810 calculated as the mean absorbance of the negative controls plus three standard deviation
811 on the same ELISA plate. Supernatant with absorbance values below the C.O were
812 classified as negative, while those with values above the C.O were considered positive.

813 **Antigen-specific ELISA**

814 Half-area High binding ELISA 96-well microplates (Corning) were coated with 30 µL per
815 well using 4µg/ml of the Spike-antigen (Wuhan, Delta, Beta, Gamma and Omicron BA2),
816 produced as previously described (56) or 1µg/ml of available RBD or 1µg/ml of NTD in
817 PBS 1x incubated overnight 4°C. In the next day, plates were blocked with 150µl of
818 blocking buffer (PBS 1x with 1% of BSA) for 1h at RT. The blocking buffer was
819 removed, and supernatants were plated diluted 1:2 using blocking buffer in 30µl volume
820 for 2h at RT. For experiments designed to quantify anti-Spike IgG secreted in SCC
821 supernatants, a standard curve was prepared using serial 1:3 dilutions of an anti-Spike
822 (Wuhan) human IgG monoclonal antibody (CZmAb) of known concentration. The plates
823 were washed five times with PBS 1x. We used an IgG conjugated with HRP as a
824 secondary antibody using a concentration of 1:4000 dilution in blocking buffer in 30µl per
825 well. The plates were washed as described above and developed with 30 µL of TMB
826 (3,3',5,5-tetramethylbenzidine) (Scienco, Brazil). The reaction was stopped with 30 µL of
827 1 N HCl, and the optical density (O.D.) was read at 450 nm with 655 nm background
828 compensation in a microplate reader (BioRad). To maximize our resources, we performed
829 the antigen-specific ELISA assays using half-area ELISA plates, which allowed us to save
830 the supernatant and conduct more assays. For the culture supernatants, Positive antibody
831 levels were determined based on a cut-off (C.O) value calculated as the mean absorbance
832 of the negative controls (NB21 culture supernatants without B cells) plus three standard
833 deviation on the same ELISA plate. Samples with absorbance values below the C.O were
834 classified as negative, while those with values above the C.O were considered positive.

835 **Production of SARS-CoV-2 variant pseudo-typed viruses and pseudovirus**
836 **neutralization assays**

837 SARS-CV-2 encoding plasmids: pcDNA3.1-SARS-CoV-2-S (Wuhan) was a gift from
838 Thomas Gallagher (57); pcDNA3.3_CoV2_P1 (Gamma), B.1.617.2 (Delta), XBB, and
839 BQ.1 were gifts from David Nemazee (58); pcDNA3.1-CoV2-Omicron BA.1 spike was a
840 gift from Ben Murrell (59). Plasmids encoding the WT (Wuhan) SARS-CoV-2 spike,
841 VOCs (Delta and P.1 Gamma) spikes and VOC Omicron sub-lineage spikes (Ba.1; Ba.2;
842 XBB; BQ.1) were transfected with Lipofectamin 3000 (Thermo) in Hek-293T cells and
843 24 hours later infected with a VSV-G pseudo-typed ΔG-luciferase (G*ΔG-luciferase) with
844 a multiplicity of infection of 5 for 2 h before washing the cells with 1×PBS.
845 Transfected/infected cells were incubated with fresh DMEM with 5% FCS. The next day,
846 transfection/infection supernatants were collected and clarified by centrifugation at 300g
847 for 10 min before filtration through a 0.45µm filter. SARS-CoV-2 pseudotyped ΔG-
848 luciferase viruses were titrated in Vero E6 cells and aliquots stored at −80°C.

849 Neutralization assays were performed by incubating pseudoviruses with serial dilutions of
850 sera or mAbs present in the supernatants from SCC monoclonal antibodies and scored by
851 the reduction in luciferase gene expression. In brief, Vero E6 cells were seeded in a white
852 96-well plate at a concentration of 2×10^4 cells per well. Pseudoviruses were incubated the
853 next day with serial dilutions of the test samples in triplicate for 30 min at 37°C. The
854 mixture was added to cultured cells and incubated for an additional 24 h. The
855 luminescence was measured by Luciferase Assay System (Promega). IC_{50} was defined as
856 the dilution at which the relative light units were reduced by 50% compared with the virus
857 control wells (virus + cells) after subtraction of the background in the control groups with
858 cells only. The IC_{50} values were calculated using nonlinear regression in GraphPad Prism.

859 **Immunoglobulin sequencing from single cell cultures**

860 To obtain single cell lysates, at day 6-7 post SCC, MBC were harvested from co-culture
861 96 well plates, centrifuged and suspended in 10 µL of TCL buffer (Qiagen) containing 1%
862 2-mercaptoethanol (60). Cell lysate plates were immediately frozen and kept at -80ºC for
863 mRNA preservation. RNAClean XP (Beckman Coulter) was used to purify mRNA
864 following the manufacturer's instructions. cDNA was synthesized with 25 pmol Oligo-dT
865 primer and 50 U of Superscript III reverse transcriptase (Invitrogen) in the presence of 4 U
866 RNAsin (Promega). Reverse transcription was carried out at 42ºC for 10 min, 25ºC for 10
867 min, 50ºC for 60 min and 94ºC for 5 min (7). cDNA was stored at -20ºC and variable
868 region from heavy and light chains were amplified using 4µL cDNA and primers
869 presented in **Supplementary Table II** (61). PCR reaction was performed with 1.25 U/
870 reaction of GoTaq Flexi DNA Polymerase (Promega) in the presence of 25 pmol primers,
871 0.2 mM dNTPs and 2 mM $MgCl_2$, as suggested by the manufacturer. Cycle conditions
872 were adapted from a previously published study (61), consisting of: 2 min at 94ºC, 4
873 cycles of 30 s at 94ºC, 30s at 50ºC and 2 min at 72ºC, followed by 8 cycles of 30 s at
874 94ºC, 30 s at 55ºC and 2 min at 72ºC and 28 cycles of 30 s 94ºC, 30 s 60ºC and 2 min at
875 72ºC. Final extension was performed at 72ºC for 10 min. Heavy and light chain PCR
876 products were purified with ExoSAP-IT (Invitrogen) according to thes manufacturer's
877 instructions and sequenced with 3.2 pmol of the reverse primer. Sanger Sequencing were
878 performed by the PSEQDNA-UFRJ facility, Biophysics Institute, Federal University of
879 Rio de Janeiro.

880 **Analysis of immunoglobulin sequences**

881 Obtained sequences were converted to fasta file and submitted to gene annotation using
882 IMGT/HighV-QUEST tool (62), in some cases Vbase 2 (63) and IgBLAST were used for
883 confirmation. VH, DH, JH, VK, VL, JK and JL gene segments were annotated, and the
884 number of nucleotide mismatch mutations were calculated. The human V genes usage of
885 the antibodies from this study were analyzed as described by Agudelo et al (25). Briefly,
886 the frequency distributions of human V genes in anti-SARS-CoV-2 antibodies compared
887 to 131,284,220 IgH and IgL sequences generated by Soto et al. (64) and downloaded from
888 cAb-Rep (65), a database of human shared BCR clonotypes available at https://cab-
889 rep.c2b2. columbia.edu/. The two-tailed t test with unequal variance was used to compare
890 the frequency distributions R of human V genes of anti-SARS-CoV-2 antibodies from this
891 study to Sequence Read Archive SRP01097039. CDR-H3 analyses were performed as
892 previously described (66). CDRH3 logograms were plotted using the online tool
893 https://weblogo.berkeley.edu/logo.cgi (67). Average hydrophobicity of CDR-H3 was
894 calculated as previously described (68).

895 **Antibody expression and purification**

896 The VH and VL antibody sequences of LBL01 and LBL02 were ordered as gBlocks
897 (Integrated DNA Technologies) and cloned by Gibson assembly (New England Biolabs)
898 into a customized pcDNA 3.4 vector containing a human IgG1 Fc region. VH and VL
899 plasmids were mixed at 1:2 ratio and were transfected into Expi293F cells (Thermo Fisher
900 Scientific), which were cultured at 37 °C and 8% CO2 for 6 days, then harvested,
901 centrifuged 4500 x g for 20 min. Antibodies were isolated from filtered (0.22µm)
902 supernatants using Protein G Plus Agarose (Pierce Thermo Fisher Scientific) affinity
903 chromatography, washed with 20 column volumes of PBS, eluted with 150 mM glycine-
904 HCl pH 2.7, and neutralized with 1 M Tris-HCl pH 8.0. The antibodies were buffer
905 exchanged into PBS and concentrated using Pierce™ Protein Concentrators PES 30.000
906 MWCO centrifugal spin columns (Thermo Fisher Scientific).

907 ***In silico* analysis of antibody binding**

908 Antibodies variable domain sequences were modeled with the ABodyBuilder2 module of
909 the ImmuneBuilder program and validated with QMEANDisCo (69, 70). Epitope
910 prediction was performed through blind docking assays using ClusPro antibody mode
911 (71). Prior the submission to ClusPro, residue charges were adjusted to pH 7.4 using
912 PDB2PQR (72). Spike structures from 10 VOCs were recovered from the Protein Data
913 Bank using the IDs: 6VYB (Wuhan); 8DLI (Alpha); 8DLL (Beta); 8DLO (Gamma);
914 7W9E (Delta); 7XO5 (Omicron BA.1); 8XZH (BA.1.1.529); 7XOA (BA.2); 7XIY
915 (BA.3); 7XNQ (BA.4/5). The lowest-energy complex from each docking run was
916 obtained, and the complexes were aligned in PyMOL to check for convergent binding
917 poses (73). The interacting amino acids were identified and used as active residues in an
918 information-driven docking step using HADDOCK2.4 and the Spike protein (PDB ID:
919 6VSB), with the aim of refining the antibody-antigen interface (74, 75). The results were
920 assessed based on cluster size, buried surface area, and HADDOCK score. Moreover,
921 binding energy was estimated using the PRODIGY webserver and protein-protein
922 interactions were identified with PDBSum (76, 77).

923 A final validation step applied heated Molecular Dynamics (MD) to assess the
924 thermostability of the HADDOCK-generated complexes, distinguishing true binding poses
925 from decoys (78). Briefly, AmberTools19 was used to insert the complexes into a
926 truncated octahedral box which was solvated with SPC/E water and adjusted to 0.15 M
927 NaCl concentration. The energy of the systems was minimized. Them, they were heated to
928 an initial temperature of 310 K and equilibrated in two subsequent steps prior to a 70 ns
929 production run. The temperature increased to 330, 360, and 390 K at 30, 42.5, and 55 ns,
930 respectively. All simulation steps were conducted in Amber18, and the trajectories were
931 analyzed in *cpptraj* to evaluate the interface RMSD using the cut-off of 5 Å to identify
932 stable poses. Three replicates of 150-ns regular MD simulations were ran using the
933 validated complexes at the temperature of 310 K. 100 frames from the last 50 ns were
934 used to extract the binding free energy (ΔG_{bind}) of the antibody-antigen complexes through
935 MM/GBSA analysis implemented in the MMPBSA.py application (79).

936 **Statistical analysis**

937 Statistical analyses were performed using GraphPad Prism 10.0 software. Using a
938 statistical model based on the Poisson distribution, the percentage of negative cultures
939 obtained in ELISA assays of LDA cultures, plotted as a function of the number of cells per
940 well, allowed estimation of the frequency of Ig-secreting B cells responsive to LPS
941 stimulation and the frequency of Ig-secreting B cells with specific reactivity to a given
942 antigen (18, 19, 80). Tests were chosen according to the type of variable and indicated in
943 each result. Results with $P > 0.05$ were considered significant.

References

1. A. L. Phelan, R. Katz, L. O. Gostin, The Novel Coronavirus Originating in Wuhan, China: Challenges for Global Health Governance. *JAMA* **323**, 709-710 (2020).
2. J. W. Yewdell, Antigenic drift: Understanding COVID-19. *Immunity* **54**, 2681-2687 (2021).
3. T. Kurosaki, K. Kometani, W. Ise, Memory B cells. *Nat Rev Immunol* **15**, 149-159 (2015).
4. I. Moran, A. Nguyen, W. H. Khoo, D. Butt, K. Bourne, C. Young, J. R. Hermes, M. Biro, G. Gracie, C. S. Ma, C. M. L. Munier, F. Luciani, J. Zaunders, A. Parker, A. D. Kelleher, S. G. Tangye, P. I. Croucher, R. Brink, M. N. Read, T. G. Phan, Memory B cells are reactivated in subcapsular proliferative foci of lymph nodes. *Nat Commun* **9**, 3372 (2018).
5. N. L. Bernasconi, E. Traggiai, A. Lanzavecchia, Maintenance of serological memory by polyclonal activation of human memory B cells. *Science* **298**, 2199-2202 (2002).
6. D. Hou, C. Chen, E. J. Seely, S. Chen, Y. Song, High-Throughput Sequencing-Based Immune Repertoire Study during Infectious Disease. *Front Immunol* **7**, 336 (2016).
7. T. Tiller, E. Meffre, S. Yurasov, M. Tsuiji, M. C. Nussenzweig, H. Wardemann, Efficient generation of monoclonal antibodies from single human B cells by single cell RT-PCR and expression vector cloning. *J Immunol Methods* **329**, 112-124 (2008).
8. D. Pinna, D. Corti, D. Jarrossay, F. Sallusto, A. Lanzavecchia, Clonal dissection of the human memory B-cell repertoire following infection and vaccination. *Eur J Immunol* **39**, 1260-1270 (2009).
9. T. Nojima, K. Haniuda, T. Moutai, M. Matsudaira, S. Mizokawa, I. Shiratori, T. Azuma, D. Kitamura, In-vitro derived germinal centre B cells differentially generate memory B or plasma cells in vivo. *Nat Commun* **2**, 465 (2011).
10. A. M. Vale, J. B. Foote, A. Granato, Y. Zhuang, R. M. Pereira, U. G. Lopes, M. Bellio, P. D. Burrows, H. W. Schroeder, Jr., A. Nobrega, A rapid and quantitative method for the evaluation of V gene usage, specificities and the clonal size of B cell repertoires. *J Immunol Methods* **376**, 143-149 (2012).
11. A. Watanabe, K. R. McCarthy, M. Kuraoka, A. G. Schmidt, Y. Adachi, T. Onodera, K. Tonouchi, T. M. Caradonna, G. Bajic, S. Song, C. E. McGee, G. D. Sempowski, F. Feng, P. Urick, T. B. Kepler, Y. Takahashi, S. C. Harrison, G. Kelsoe, Antibodies to a Conserved Influenza Head Interface Epitope Protect by an IgG Subtype-Dependent Mechanism. *Cell* **177**, 1124-1135 e1116 (2019).
12. K. Y. Su, A. Watanabe, C. H. Yeh, G. Kelsoe, M. Kuraoka, Efficient Culture of Human Naive and Memory B Cells for Use as APCs. *J Immunol* **197**, 4163-4176 (2016).
13. K. R. McCarthy, A. Watanabe, M. Kuraoka, K. T. Do, C. E. McGee, G. D. Sempowski, T. B. Kepler, A. G. Schmidt, G. Kelsoe, S. C. Harrison, Memory B Cells that Cross-React with Group 1 and Group 2 Influenza A Viruses Are Abundant in Adult Human Repertoires. *Immunity* **48**, 174-184 e179 (2018).
14. S. J. Zost, P. Gilchuk, R. E. Chen, J. B. Case, J. X. Reidy, A. Trivette, R. S. Nargi, R. E. Sutton, N. Suryadevara, E. C. Chen, E. Binshtein, S. Shrihari, M. Ostrowski, H. Y. Chu, J. E. Didier, K. W. MacRenaris, T. Jones, S. Day, L. Myers, F. Eun-Hyung Lee, D. C. Nguyen, I. Sanz, D. R. Martinez, P. W. Rothlauf, L. M. Bloyet, S. P. J. Whelan, R. S. Baric, L. B. Thackray, M. S. Diamond, R. H. Carnahan, J. E. Crowe, Jr., Rapid isolation and profiling of a diverse panel of human monoclonal antibodies targeting the SARS-CoV-2 spike protein. *Nat Med* **26**, 1422-1427 (2020).
15. L. S. Collins, K. Dorshkind, A stromal cell line from myeloid long-term bone marrow cultures can support myelopoiesis and B lymphopoiesis. *J Immunol* **138**, 1082-1087 (1987).

16. M. Kuraoka, A. G. Schmidt, T. Nojima, F. Feng, A. Watanabe, D. Kitamura, S. C. Harrison, T. B. Kepler, G. Kelsoe, Complex Antigens Drive Permissive Clonal Selection in Germinal Centers. *Immunity* **44**, 542-552 (2016).
17. Y. M. Adzavon, P. Zhao, B. Lv, M. Liu, X. Zhang, F. Xie, L. Yang, L. Shang, M. Zhang, Q. Li, X. Ma, TLR7 and TLR8 agonist resiquimod (R848) differently regulates MIF expression in cells and organs. *Cytokine* **97**, 156-166 (2017).
18. J. Andersson, A. Coutinho, W. Lernhardt, F. Melchers, Clonal growth and maturation to immunoglobulin secretion in vitro of every growth-inducible B lymphocyte. *Cell* **10**, 27-34 (1977).
19. C. Taswell, Limiting dilution assays for the determination of immunocompetent cell frequencies. I. Data analysis. *J Immunol* **126**, 1614-1619 (1981).
20. L. H. Nguyen, D. A. Drew, A. D. Joshi, C. G. Guo, W. Ma, R. S. Mehta, D. R. Sikavi, C. H. Lo, S. Kwon, M. Song, L. A. Mucci, M. J. Stampfer, W. C. Willett, A. H. Eliassen, J. E. Hart, J. E. Chavarro, J. W. Rich-Edwards, R. Davies, J. Capdevila, K. A. Lee, M. N. Lochlainn, T. Varsavsky, M. S. Graham, C. H. Sudre, M. J. Cardoso, J. Wolf, S. Ourselin, C. J. Steves, T. D. Spector, A. T. Chan, Risk of COVID-19 among frontline healthcare workers and the general community: a prospective cohort study. *medRxiv*, (2020).
21. X. Chi, R. Yan, J. Zhang, G. Zhang, Y. Zhang, M. Hao, Z. Zhang, P. Fan, Y. Dong, Y. Yang, Z. Chen, Y. Guo, J. Zhang, Y. Li, X. Song, Y. Chen, L. Xia, L. Fu, L. Hou, J. Xu, C. Yu, J. Li, Q. Zhou, W. Chen, A neutralizing human antibody binds to the N-terminal domain of the Spike protein of SARS-CoV-2. *Science* **369**, 650-655 (2020).
22. M. A. Diaz-Salinas, A. Jain, N. D. Durham, J. B. Munro, Single-molecule imaging reveals allosteric stimulation of SARS-CoV-2 spike receptor binding domain by host sialic acid. *Sci Adv* **10**, eadk4920 (2024).
23. F. Amanat, M. Thapa, T. Lei, S. M. S. Ahmed, D. C. Adelsberg, J. M. Carreno, S. Strohmeier, A. J. Schmitz, S. Zafar, J. Q. Zhou, W. Rijnink, H. Alshammary, N. Borcherding, A. G. Reiche, K. Srivastava, E. M. Sordillo, H. van Bakel, I. Personalized Virology, J. S. Turner, G. Bajic, V. Simon, A. H. Ellebedy, F. Krammer, SARS-CoV-2 mRNA vaccination induces functionally diverse antibodies to NTD, RBD, and S2. *Cell* **184**, 3936-3948 e3910 (2021).
24. W. N. Voss, Y. J. Hou, N. V. Johnson, G. Delidakis, J. E. Kim, K. Javanmardi, A. P. Horton, F. Bartzoka, C. J. Paresi, Y. Tanno, C. W. Chou, S. A. Abbasi, W. Pickens, K. George, D. R. Boutz, D. M. Towers, J. R. McDaniel, D. Billick, J. Goike, L. Rowe, D. Batra, J. Pohl, J. Lee, S. Gangappa, S. Sambhara, M. Gadush, N. Wang, M. D. Person, B. L. Iverson, J. D. Gollihar, J. M. Dye, A. S. Herbert, I. J. Finkelstein, R. S. Baric, J. S. McLellan, G. Georgiou, J. J. Lavinder, G. C. Ippolito, Prevalent, protective, and convergent IgG recognition of SARS-CoV-2 non-RBD spike epitopes. *Science* **372**, 1108-1112 (2021).
25. M. Agudelo, F. Muecksch, D. Schaefer-Babajew, A. Cho, J. DaSilva, E. Bednarski, V. Ramos, T. Y. Oliveira, M. Cipolla, A. Gazumyan, S. Zong, D. A. S. Rodrigues, G. S. Lira, L. Conde, R. S. Aguiar, O. C. Ferreira, A. Tanuri, K. C. Affonso, R. M. Galliez, T. Castineiras, J. Echevarria-Lima, M. T. Bozza, A. M. Vale, P. D. Bieniasz, T. Hatziioannou, M. C. Nussenzweig, Plasma and memory antibody responses to Gamma SARS-CoV-2 provide limited cross-protection to other variants. *J Exp Med* **219**, (2022).
26. D. F. Robbiani, C. Gaebler, F. Muecksch, J. C. C. Lorenzi, Z. Wang, A. Cho, M. Agudelo, C. O. Barnes, A. Gazumyan, S. Finkin, T. Hagglof, T. Y. Oliveira, C. Viant, A. Hurley, H. H. Hoffmann, K. G. Millard, R. G. Kost, M. Cipolla, K. Gordon, F. Bianchini, S. T. Chen, V. Ramos, R. Patel, J. Dizon, I. Shimeliovich, P. Mendoza, H. Hartweger, L. Nogueira, M. Pack, J. Horowitz, F. Schmidt, Y. Weisblum, E. Michailidis, A. W. Ashbrook, E. Waltari, J. E. Pak, K. E. Huey-Tubman, N. Koranda, P. R. Hoffman, A. P. West, Jr., C. M. Rice, T. Hatziioannou, P. J. Bjorkman, P. D. Bieniasz, M. Caskey, M. C. Nussenzweig, Convergent

1042 antibody responses to SARS-CoV-2 in convalescent individuals. *Nature* **584**, 437-442
1043 (2020).
1044 27. Y. Wang, M. Yuan, H. Lv, J. Peng, I. A. Wilson, N. C. Wu, A large-scale systematic survey
1045 reveals recurring molecular features of public antibody responses to SARS-CoV-2.
1046 *Immunity* **55**, 1105-1117 e1104 (2022).
1047 28. N. S. Lima, M. Musayev, T. S. Johnston, D. A. Wagner, A. R. Henry, L. Wang, E. S. Yang,
1048 Y. Zhang, K. Birungi, W. P. Black, S. O'Dell, S. D. Schmidt, D. Moon, C. G. Lorang, B.
1049 Zhao, M. Chen, K. L. Boswell, J. Roberts-Torres, R. L. Davis, L. Peyton, S. R. Narpala, S.
1050 O'Connell, L. Serebryannyy, J. Wang, A. Schrager, C. A. Talana, G. Shimberg, K. Leung,
1051 W. Shi, R. Khashab, A. Biber, T. Zilberman, J. Rhein, S. Vetter, A. Ahmed, L. Novik, A.
1052 Widge, I. Gordon, M. Guech, I. T. Teng, E. Phung, T. J. Ruckwardt, A. Pegu, J. Misasi, N.
1053 A. Doria-Rose, M. Gaudinski, R. A. Koup, P. D. Kwong, A. B. McDermott, S. Amit, T. W.
1054 Schacker, I. Levy, J. R. Mascola, N. J. Sullivan, C. A. Schramm, D. C. Douek, Primary
1055 exposure to SARS-CoV-2 variants elicits convergent epitope specificities, immunoglobulin
1056 V gene usage and public B cell clones. *Nat Commun* **13**, 7733 (2022).
1057 29. W. T. He, R. Musharrafieh, G. Song, K. Dueker, L. V. Tse, D. R. Martinez, A. Schafer, S.
1058 Callaghan, P. Yong, N. Beutler, J. L. Torres, R. M. Volk, P. Zhou, M. Yuan, H. Liu, F.
1059 Anzanello, T. Capozzola, M. Parren, E. Garcia, S. A. Rawlings, D. M. Smith, I. A. Wilson,
1060 Y. Safonova, A. B. Ward, T. F. Rogers, R. S. Baric, L. E. Gralinski, D. R. Burton, R.
1061 Andrabi, Targeted isolation of diverse human protective broadly neutralizing antibodies
1062 against SARS-like viruses. *Nat Immunol* **23**, 960-970 (2022).
1063 30. M. Yuan, H. Liu, N. C. Wu, C. D. Lee, X. Zhu, F. Zhao, D. Huang, W. Yu, Y. Hua, H. Tien,
1064 T. F. Rogers, E. Landais, D. Sok, J. G. Jardine, D. R. Burton, I. A. Wilson, Structural basis
1065 of a shared antibody response to SARS-CoV-2. *Science* **369**, 1119-1123 (2020).
1066 31. Y. Cao, B. Su, X. Guo, W. Sun, Y. Deng, L. Bao, Q. Zhu, X. Zhang, Y. Zheng, C. Geng,
1067 X. Chai, R. He, X. Li, Q. Lv, H. Zhu, W. Deng, Y. Xu, Y. Wang, L. Qiao, Y. Tan, L. Song,
1068 G. Wang, X. Du, N. Gao, J. Liu, J. Xiao, X. D. Su, Z. Du, Y. Feng, C. Qin, C. Qin, R. Jin,
1069 X. S. Xie, Potent Neutralizing Antibodies against SARS-CoV-2 Identified by High-
1070 Throughput Single-Cell Sequencing of Convalescent Patients' B Cells. *Cell* **182**, 73-84 e16
1071 (2020).
1072 32. S. A. Clark, L. E. Clark, J. Pan, A. Coscia, L. G. A. McKay, S. Shankar, R. I. Johnson, V.
1073 Brusic, M. C. Choudhary, J. Regan, J. Z. Li, A. Griffiths, J. Abraham, SARS-CoV-2
1074 evolution in an immunocompromised host reveals shared neutralization escape
1075 mechanisms. *Cell* **184**, 2605-2617 e2618 (2021).
1076 33. S. I. Kim, J. Noh, S. Kim, Y. Choi, D. K. Yoo, Y. Lee, H. Lee, J. Jung, C. K. Kang, K. H.
1077 Song, P. G. Choe, H. B. Kim, E. S. Kim, N. J. Kim, M. W. Seong, W. B. Park, M. D. Oh,
1078 S. Kwon, J. Chung, Stereotypic neutralizing V(H) antibodies against SARS-CoV-2 spike
1079 protein receptor binding domain in patients with COVID-19 and healthy individuals. *Sci*
1080 *Transl Med* **13**, (2021).
1081 34. T. J. C. Tan, M. Yuan, K. Kuzelka, G. C. Padron, J. R. Beal, X. Chen, Y. Wang, J. Rivera-
1082 Cardona, X. Zhu, B. M. Stadtmueller, C. B. Brooke, I. A. Wilson, N. C. Wu, Sequence
1083 signatures of two IGHV3-53/3-66 public clonotypes to SARS-CoV-2 receptor binding
1084 domain. *bioRxiv*, (2021).
1085 35. M. Yuan, H. Liu, N. C. Wu, I. A. Wilson, Recognition of the SARS-CoV-2 receptor binding
1086 domain by neutralizing antibodies. *Biochem Biophys Res Commun* **538**, 192-203 (2021).
1087 36. Q. Zhang, B. Ju, J. Ge, J. F. Chan, L. Cheng, R. Wang, W. Huang, M. Fang, P. Chen, B.
1088 Zhou, S. Song, S. Shan, B. Yan, S. Zhang, X. Ge, J. Yu, J. Zhao, H. Wang, L. Liu, Q. Lv,
1089 L. Fu, X. Shi, K. Y. Yuen, L. Liu, Y. Wang, Z. Chen, L. Zhang, X. Wang, Z. Zhang, Potent
1090 and protective IGHV3-53/3-66 public antibodies and their shared escape mutant on the
1091 spike of SARS-CoV-2. *Nat Commun* **12**, 4210 (2021).

1092 37. P. Tong, A. Gautam, I. W. Windsor, M. Travers, Y. Chen, N. Garcia, N. B. Whiteman, L.
1093 G. A. McKay, N. Storm, L. E. Malsick, A. N. Honko, F. J. N. Lelis, S. Habibi, S. Jenni, Y.
1094 Cai, L. J. Rennick, W. P. Duprex, K. R. McCarthy, C. L. Lavine, T. Zuo, J. Lin, A. Zuiani,
1095 J. Feldman, E. A. MacDonald, B. M. Hauser, A. Griffths, M. S. Seaman, A. G. Schmidt, B.
1096 Chen, D. Neuberg, G. Bajic, S. C. Harrison, D. R. Wesemann, Memory B cell repertoire for
1097 recognition of evolving SARS-CoV-2 spike. *Cell* **184**, 4969-4980 e4915 (2021).
1098 38. M. F. Jennewein, A. J. MacCamy, N. R. Akins, J. Feng, L. J. Homad, N. K. Hurlburt, E.
1099 Seydoux, Y. H. Wan, A. B. Stuart, V. V. Edara, K. Floyd, A. Vanderheiden, J. R. Mascola,
1100 N. Doria-Rose, L. Wang, E. S. Yang, H. Y. Chu, J. L. Torres, G. Ozorowski, A. B. Ward,
1101 R. E. Whaley, K. W. Cohen, M. Pancera, M. J. McElrath, J. A. Englund, A. Finzi, M. S.
1102 Suthar, A. T. McGuire, L. Stamatatos, Isolation and characterization of cross-neutralizing
1103 coronavirus antibodies from COVID-19+ subjects. *Cell Rep* **36**, 109353 (2021).
1104 39. C. Kreer, M. Zehner, T. Weber, M. S. Ercanoglu, L. Gieselmann, C. Rohde, S. Halwe, M.
1105 Korenkov, P. Schommers, K. Vanshylla, V. Di Cristanziano, H. Janicki, R. Brinker, A.
1106 Ashurov, V. Krahling, A. Kupke, H. Cohen-Dvashi, M. Koch, J. M. Eckert, S. Lederer, N.
1107 Pfeifer, T. Wolf, M. Vehreschild, C. Wendtner, R. Diskin, H. Gruell, S. Becker, F. Klein,
1108 Longitudinal Isolation of Potent Near-Germline SARS-CoV-2-Neutralizing Antibodies
1109 from COVID-19 Patients. *Cell* **182**, 843-854 e812 (2020).
1110 40. D. Li, R. J. Edwards, K. Manne, D. R. Martinez, A. Schafer, S. M. Alam, K. Wiehe, X. Lu,
1111 R. Parks, L. L. Sutherland, T. H. Oguin, 3rd, C. McDanal, L. G. Perez, K. Mansouri, S. M.
1112 C. Gobeil, K. Janowska, V. Stalls, M. Kopp, F. Cai, E. Lee, A. Foulger, G. E. Hernandez,
1113 A. Sanzone, K. Tilahun, C. Jiang, L. V. Tse, K. W. Bock, M. Minai, B. M. Nagata, K.
1114 Cronin, V. Gee-Lai, M. Deyton, M. Barr, T. Von Holle, A. N. Macintyre, E. Stover, J.
1115 Feldman, B. M. Hauser, T. M. Caradonna, T. D. Scobey, W. Rountree, Y. Wang, M. A.
1116 Moody, D. W. Cain, C. T. DeMarco, T. N. Denny, C. W. Woods, E. W. Petzold, A. G.
1117 Schmidt, I. T. Teng, T. Zhou, P. D. Kwong, J. R. Mascola, B. S. Graham, I. N. Moore, R.
1118 Seder, H. Andersen, M. G. Lewis, D. C. Montefiori, G. D. Sempowski, R. S. Baric, P.
1119 Acharya, B. F. Haynes, K. O. Saunders, In vitro and in vivo functions of SARS-CoV-2
1120 infection-enhancing and neutralizing antibodies. *Cell* **184**, 4203-4219 e4232 (2021).
1121 41. M. Sakharkar, C. G. Rappazzo, W. F. Wieland-Alter, C. L. Hsieh, D. Wrapp, E. S. Esterman,
1122 C. I. Kaku, A. Z. Wec, J. C. Geoghegan, J. S. McLellan, R. I. Connor, P. F. Wright, L. M.
1123 Walker, Prolonged evolution of the human B cell response to SARS-CoV-2 infection. *Sci*
1124 *Immunol* **6**, (2021).
1125 42. A. K. Wheatley, J. A. Juno, J. J. Wang, K. J. Selva, A. Reynaldi, H. X. Tan, W. S. Lee, K.
1126 M. Wragg, H. G. Kelly, R. Esterbauer, S. K. Davis, H. E. Kent, F. L. Mordant, T. E. Schlub,
1127 D. L. Gordon, D. S. Khoury, K. Subbarao, D. Cromer, T. P. Gordon, A. W. Chung, M. P.
1128 Davenport, S. J. Kent, Evolution of immune responses to SARS-CoV-2 in mild-moderate
1129 COVID-19. *Nat Commun* **12**, 1162 (2021).
1130 43. B. Briney, A. Inderbitzin, C. Joyce, D. R. Burton, Commonality despite exceptional
1131 diversity in the baseline human antibody repertoire. *Nature* **566**, 393-397 (2019).
1132 44. L. Li, X. Chen, Z. Wang, Y. Li, C. Wang, L. Jiang, T. Zuo, Breakthrough infection elicits
1133 hypermutated IGHV3-53/3-66 public antibodies with broad and potent neutralizing activity
1134 against SARS-CoV-2 variants including the emerging EG.5 lineages. *PLoS Pathog* **19**,
1135 e1011856 (2023).
1136 45. H. Yuuki, T. Itamiya, Y. Nagafuchi, M. Ota, K. Fujio, B cell receptor repertoire
1137 abnormalities in autoimmune disease. *Front Immunol* **15**, 1326823 (2024).
1138 46. H. B. Shah, K. Smith, J. D. Wren, C. F. Webb, J. D. Ballard, R. L. Bourn, J. A. James, M.
1139 L. Lang, Insights From Analysis of Human Antigen-Specific Memory B Cell Repertoires.
1140 *Front Immunol* **9**, 3064 (2018).

1141 47. L. Piccoli, Y. J. Park, M. A. Tortorici, N. Czudnochowski, A. C. Walls, M. Beltramello, C.
1142 Silacci-Fregni, D. Pinto, L. E. Rosen, J. E. Bowen, O. J. Acton, S. Jaconi, B. Guarino, A.
1143 Minola, F. Zatta, N. Sprugasci, J. Bassi, A. Peter, A. De Marco, J. C. Nix, F. Mele, S. Jovic,
1144 B. F. Rodriguez, S. V. Gupta, F. Jin, G. Piumatti, G. Lo Presti, A. F. Pellanda, M.
1145 Biggiogero, M. Tarkowski, M. S. Pizzuto, E. Cameroni, C. Havenar-Daughton, M. Smithey,
1146 D. Hong, V. Lepori, E. Albanese, A. Ceschi, E. Bernasconi, L. Elzi, P. Ferrari, C. Garzoni,
1147 A. Riva, G. Snell, F. Sallusto, K. Fink, H. W. Virgin, A. Lanzavecchia, D. Corti, D. Veesler,
1148 Mapping Neutralizing and Immunodominant Sites on the SARS-CoV-2 Spike Receptor-
1149 Binding Domain by Structure-Guided High-Resolution Serology. *Cell* **183**, 1024-1042
1150 e1021 (2020).
1151 48. J. L. M. Law, M. Logan, M. A. Joyce, A. Landi, D. Hockman, K. Crawford, J. Johnson, G.
1152 LaChance, H. A. Saffran, J. Shields, E. Hobart, R. Brassard, E. Arutyunova, K. Pabbaraju,
1153 M. Croxen, G. Tipples, M. J. Lemieux, D. L. Tyrrell, M. Houghton, SARS-COV-2
1154 recombinant Receptor-Binding-Domain (RBD) induces neutralizing antibodies against
1155 variant strains of SARS-CoV-2 and SARS-CoV-1. *Vaccine* **39**, 5769-5779 (2021).
1156 49. G. Cerutti, Y. Guo, T. Zhou, J. Gorman, M. Lee, M. Rapp, E. R. Reddem, J. Yu, F. Bahna,
1157 J. Bimela, Y. Huang, P. S. Katsamba, L. Liu, M. S. Nair, R. Rawi, A. S. Olia, P. Wang, B.
1158 Zhang, G. Y. Chuang, D. D. Ho, Z. Sheng, P. D. Kwong, L. Shapiro, Potent SARS-CoV-2
1159 neutralizing antibodies directed against spike N-terminal domain target a single supersite.
1160 *Cell Host Microbe* **29**, 819-833 e817 (2021).
1161 50. S. Thakur, S. Sasi, S. G. Pillai, A. Nag, D. Shukla, R. Singhal, S. Phalke, G. S. K. Velu,
1162 SARS-CoV-2 Mutations and Their Impact on Diagnostics, Therapeutics and Vaccines.
1163 *Front Med (Lausanne)* **9**, 815389 (2022).
1164 51. W. T. Harvey, A. M. Carabelli, B. Jackson, R. K. Gupta, E. C. Thomson, E. M. Harrison,
1165 C. Ludden, R. Reeve, A. Rambaut, C.-G. U. Consortium, S. J. Peacock, D. L. Robertson,
1166 SARS-CoV-2 variants, spike mutations and immune escape. *Nat Rev Microbiol* **19**, 409-
1167 424 (2021).
1168 52. D. Gupta, P. Sharma, M. Singh, M. Kumar, A. S. Ethayathulla, P. Kaur, Structural and
1169 functional insights into the spike protein mutations of emerging SARS-CoV-2 variants. *Cell*
1170 *Mol Life Sci* **78**, 7967-7989 (2021).
1171 53. M. McCallum, A. De Marco, F. A. Lempp, M. A. Tortorici, D. Pinto, A. C. Walls, M.
1172 Beltramello, A. Chen, Z. Liu, F. Zatta, S. Zepeda, J. di Iulio, J. E. Bowen, M. Montiel-Ruiz,
1173 J. Zhou, L. E. Rosen, S. Bianchi, B. Guarino, C. S. Fregni, R. Abdelnabi, S. C. Foo, P. W.
1174 Rothlauf, L. M. Bloyet, F. Benigni, E. Cameroni, J. Neyts, A. Riva, G. Snell, A. Telenti, S.
1175 P. J. Whelan, H. W. Virgin, D. Corti, M. S. Pizzuto, D. Veesler, N-terminal domain
1176 antigenic mapping reveals a site of vulnerability for SARS-CoV-2. *Cell* **184**, 2332-2347
1177 e2316 (2021).
1178 54. A. Z. Wec, D. Wrapp, A. S. Herbert, D. P. Maurer, D. Haslwanter, M. Sakharkar, R. K.
1179 Jangra, M. E. Dieterle, A. Lilov, D. Huang, L. V. Tse, N. V. Johnson, C. L. Hsieh, N. Wang,
1180 J. H. Nett, E. Champney, I. Burnina, M. Brown, S. Lin, M. Sinclair, C. Johnson, S. Pudi, R.
1181 Bortz, 3rd, A. S. Wirchnianski, E. Laudermilch, C. Florez, J. M. Fels, C. M. O'Brien, B. S.
1182 Graham, D. Nemazee, D. R. Burton, R. S. Baric, J. E. Voss, K. Chandran, J. M. Dye, J. S.
1183 McLellan, L. M. Walker, Broad neutralization of SARS-related viruses by human
1184 monoclonal antibodies. *Science* **369**, 731-736 (2020).
1185 55. C. O. Barnes, A. P. West, Jr., K. E. Huey-Tubman, M. A. G. Hoffmann, N. G. Sharaf, P. R.
1186 Hoffman, N. Koranda, H. B. Gristick, C. Gaebler, F. Muecksch, J. C. C. Lorenzi, S. Finkin,
1187 T. Hagglof, A. Hurley, K. G. Millard, Y. Weisblum, F. Schmidt, T. Hatziioannou, P. D.
1188 Bieniasz, M. Caskey, D. F. Robbiani, M. C. Nussenzweig, P. J. Bjorkman, Structures of
1189 Human Antibodies Bound to SARS-CoV-2 Spike Reveal Common Epitopes and Recurrent
1190 Features of Antibodies. *Cell* **182**, 828-842 e816 (2020).

1191 56. R. G. F. Alvim, T. M. Lima, D. A. S. Rodrigues, F. F. Marsili, V. B. T. Bozza, L. M. Higa,
1192 F. L. Monteiro, D. P. B. Abreu, I. C. Leitao, R. S. Carvalho, R. M. Galliez, T. Castineiras,
1193 L. H. Travassos, A. Nobrega, A. Tanuri, O. C. Ferreira, Jr., A. M. Vale, L. R. Castilho, From
1194 a recombinant key antigen to an accurate, affordable serological test: Lessons learnt from
1195 COVID-19 for future pandemics. *Biochem Eng J* **186**, 108537 (2022).
1196 57. E. Qing, T. Kicmal, B. Kumar, G. M. Hawkins, E. Timm, S. Perlman, T. Gallagher,
1197 Dynamics of SARS-CoV-2 Spike Proteins in Cell Entry: Control Elements in the Amino-
1198 Terminal Domains. *mBio* **12**, e0159021 (2021).
1199 58. P. Zhou, G. Song, H. Liu, M. Yuan, W. T. He, N. Beutler, X. Zhu, L. V. Tse, D. R. Martinez,
1200 A. Schafer, F. Anzanello, P. Yong, L. Peng, K. Dueker, R. Musharrafieh, S. Callaghan, T.
1201 Capozzola, O. Limbo, M. Parren, E. Garcia, S. A. Rawlings, D. M. Smith, D. Nemazee, J.
1202 G. Jardine, Y. Safonova, B. Briney, T. F. Rogers, I. A. Wilson, R. S. Baric, L. E. Gralinski,
1203 D. R. Burton, R. Andrabi, Broadly neutralizing anti-S2 antibodies protect against all three
1204 human betacoronaviruses that cause deadly disease. *Immunity* **56**, 669-686 e667 (2023).
1205 59. D. J. Sheward, C. Kim, R. A. Ehling, A. Pankow, X. Castro Dopico, R. Dyrdak, D. P.
1206 Martin, S. T. Reddy, J. Dillner, G. B. Karlsson Hedestam, J. Albert, B. Murrell,
1207 Neutralisation sensitivity of the SARS-CoV-2 omicron (B.1.1.529) variant: a cross-
1208 sectional study. *Lancet Infect Dis* **22**, 813-820 (2022).
1209 60. J. J. Trombetta, D. Gennert, D. Lu, R. Satija, A. K. Shalek, A. Regev, Preparation of Single-
1210 Cell RNA-Seq Libraries for Next Generation Sequencing. *Curr Protoc Mol Biol* **107**, 4 22
1211 21-24 22 17 (2014).
1212 61. J. R. McDaniel, B. J. DeKosky, H. Tanno, A. D. Ellington, G. Georgiou, Ultra-high-
1213 throughput sequencing of the immune receptor repertoire from millions of lymphocytes.
1214 *Nat Protoc* **11**, 429-442 (2016).
1215 62. E. Alamyar, P. Duroux, M. P. Lefranc, V. Giudicelli, IMGT((R)) tools for the nucleotide
1216 analysis of immunoglobulin (IG) and T cell receptor (TR) V-(D)-J repertoires,
1217 polymorphisms, and IG mutations: IMGT/V-QUEST and IMGT/HighV-QUEST for NGS.
1218 *Methods Mol Biol* **882**, 569-604 (2012).
1219 63. I. Retter, H. H. Althaus, R. Munch, W. Muller, VBASE2, an integrative V gene database.
1220 *Nucleic Acids Res* **33**, D671-674 (2005).
1221 64. C. Soto, R. G. Bombardi, A. Branchizio, N. Kose, P. Matta, A. M. Sevy, R. S. Sinkovits, P.
1222 Gilchuk, J. A. Finn, J. E. Crowe, Jr., High frequency of shared clonotypes in human B cell
1223 receptor repertoires. *Nature* **566**, 398-402 (2019).
1224 65. Y. Guo, K. Chen, P. D. Kwong, L. Shapiro, Z. Sheng, cAb-Rep: A Database of Curated
1225 Antibody Repertoires for Exploring Antibody Diversity and Predicting Antibody
1226 Prevalence. *Front Immunol* **10**, 2365 (2019).
1227 66. Ivanov, II, R. L. Schelonka, Y. Zhuang, G. L. Gartland, M. Zemlin, H. W. Schroeder, Jr.,
1228 Development of the expressed Ig CDR-H3 repertoire is marked by focusing of constraints
1229 in length, amino acid use, and charge that are first established in early B cell progenitors. *J*
1230 *Immunol* **174**, 7773-7780 (2005).
1231 67. G. E. Crooks, G. Hon, J. M. Chandonia, S. E. Brenner, WebLogo: a sequence logo
1232 generator. *Genome Res* **14**, 1188-1190 (2004).
1233 68. J. Kyte, R. F. Doolittle, A simple method for displaying the hydropathic character of a
1234 protein. *Journal of molecular biology* **157**, 105-132 (1982).
1235 69. B. Abanades, W. K. Wong, F. Boyles, G. Georges, A. Bujotzek, C. M. Deane,
1236 ImmuneBuilder: Deep-Learning models for predicting the structures of immune proteins.
1237 *Commun Biol* **6**, 575 (2023).
1238 70. G. Studer, C. Rempfer, A. M. Waterhouse, R. Gumienny, J. Haas, T. Schwede,
1239 QMEANDisCo-distance constraints applied on model quality estimation. *Bioinformatics*
1240 **36**, 1765-1771 (2020).

71. D. Kozakov, D. R. Hall, B. Xia, K. A. Porter, D. Padhorny, C. Yueh, D. Beglov, S. Vajda, The ClusPro web server for protein-protein docking. *Nat Protoc* **12**, 255-278 (2017).
72. T. J. Dolinsky, P. Czodrowski, H. Li, J. E. Nielsen, J. H. Jensen, G. Klebe, N. A. Baker, PDB2PQR: expanding and upgrading automated preparation of biomolecular structures for molecular simulations. *Nucleic Acids Res* **35**, W522-525 (2007).
73. L. Schrödinger, & DeLano, W. (2020).
74. R. V. Honorato, M. E. Trellet, B. Jimenez-Garcia, J. J. Schaarschmidt, M. Giulini, V. Reys, P. I. Koukos, J. Rodrigues, E. Karaca, G. C. P. van Zundert, J. Roel-Touris, C. W. van Noort, Z. Jandova, A. S. J. Melquiond, A. Bonvin, The HADDOCK2.4 web server for integrative modeling of biomolecular complexes. *Nat Protoc* **19**, 3219-3241 (2024).
75. D. Wrapp, N. Wang, K. S. Corbett, J. A. Goldsmith, C. L. Hsieh, O. Abiona, B. S. Graham, J. S. McLellan, Cryo-EM structure of the 2019-nCoV spike in the prefusion conformation. *Science* **367**, 1260-1263 (2020).
76. L. C. Xue, J. P. Rodrigues, P. L. Kastritis, A. M. Bonvin, A. Vangone, PRODIGY: a web server for predicting the binding affinity of protein-protein complexes. *Bioinformatics* **32**, 3676-3678 (2016).
77. R. A. Laskowski, PDBsum1: A standalone program for generating PDBsum analyses. *Protein Sci* **31**, e4473 (2022).
78. F. Radom, A. Pluckthun, E. Paci, Assessment of ab initio models of protein complexes by molecular dynamics. *PLoS Comput Biol* **14**, e1006182 (2018).
79. B. R. Miller, 3rd, T. D. McGee, Jr., J. M. Swails, N. Homeyer, H. Gohlke, A. E. Roitberg, MMPBSA.py: An Efficient Program for End-State Free Energy Calculations. *J Chem Theory Comput* **8**, 3314-3321 (2012).
80. G. Fazekas de St, The evaluation of limiting dilution assays. *J Immunol Methods* **49**, R11-23 (1982).

Acknowledgments

We extend our gratitude to all study participants for their time and contribution to our research. We thank the members of the Laboratório de Instrumentação Nuclear (CT - UFRJ) for their assistance with cell irradiation; the Unidade Multiusuário de Citometria - IMPG (CCS/UFRJ) team for their support with the MoFlo sorter (Dako Cytomation) and technical assistance; Ronaldo Rocha (LAGIIVIR, IMPG – UFRJ) for technical assistance. We are grateful to Dr. Garnett Kelsoe (Duke University, Durham, NC) for generously providing the NB21 feeder cells and to Victor Ramos (Laboratory of Molecular Immunology, The Rockefeller University) for sharing the human V gene database and supporting the V gene segment analysis. We thank Professor Pedro Moreno Pimentel-Coelho from the Laboratório de Neuropatologia Experimental (LINE - UFRJ). We also thank all the GIISER-Brazil members for their contributions.

Funding:

This work was partially funded by from the Global Immunology and Immune Sequencing for Epidemic Response (GIISER)-Brazil/Bill and Melinda Gates Foundation to AB and AMV; The Stavros Niarchos Foundation Institute at Rockefeller University (SNIFRU) to GDV and AMV; Instituto Serrapilheira grant to AT and AMV; and the Brazilian research funding agencies: Fundação de Amparo à Pesquisa do Estado do Rio de Janeiro (FAPERJ), Conselho Nacional de Desenvolvimento Científico e Tecnológico (CNPq), Coordenação de Aperfeiçoamento de Pessoal de Nível Superior (CAPES), Financiadora de Estudos e Projetos (FINEP) and Fundação de Amparo à Pesquisa de Minas Gerais (FAPEMIG) [APQ-00501-23, APQ-04025-23, Rede Mineira de Imunobiologicos grant

#REDE-00140-16]. L. Conde received a PhD fellowship from FAPERJ. Additional funding was provided by INOVA COVID-19/FIOCRUZ, INCT NeuroImmunomodulation, Rede de ImunoInflamação, and FOCEM/Mercosul to AB; CAPES (COMBATECovid) and ANRS | Maladies infectieuses émergentes/Inserm grant (MUCOVID- 007) grant to MTB; Corona-Ômica -CNPq/FINEP to LJC. GDV is an HHMI Investigator.

Author contributions:

Conceptualization: LC, DLO, AB and AMV
Performed experiments: LC, DLO, GM, FC, DARS, YM, and AMV
Experimental support: GMA, BG, LT, BS, PC and BM
Patient enrollment: AT, OCFJr and TMPPC,
Sample processing and storage: LC, GM, DASR, BG, JE, and MB
Spike proteins production: LRC
Pseudo neutralization assays: SSF, MSC, LJC
Antibody expression and purification: CN, MCE, MNR and LFF
In silico analysis of antibody binding: AOA and JHMS
Intellectual contribution: OCFJr, LFF, LJC, AN, GDV, CL, AB and AMV
Analyzed data: LC, DLO, GM, FC, AOA, AN, AB and AMV
Funding acquisition: AT, MTB, LFF, GDV, CL, AB and AMV
Resources: FMBO, JE, MB
Writing—original draft: LC, DLO and AMV
Writing—review & editing: LC, DLO, AOA, FMBO, FJC, LFF, AN, GDV, CL, AB and AMV

Competing interests:
Authors declare that they have no competing interests.

Data and materials availability: All data are available in the main text or the supplementary materials.

Figures and Tables

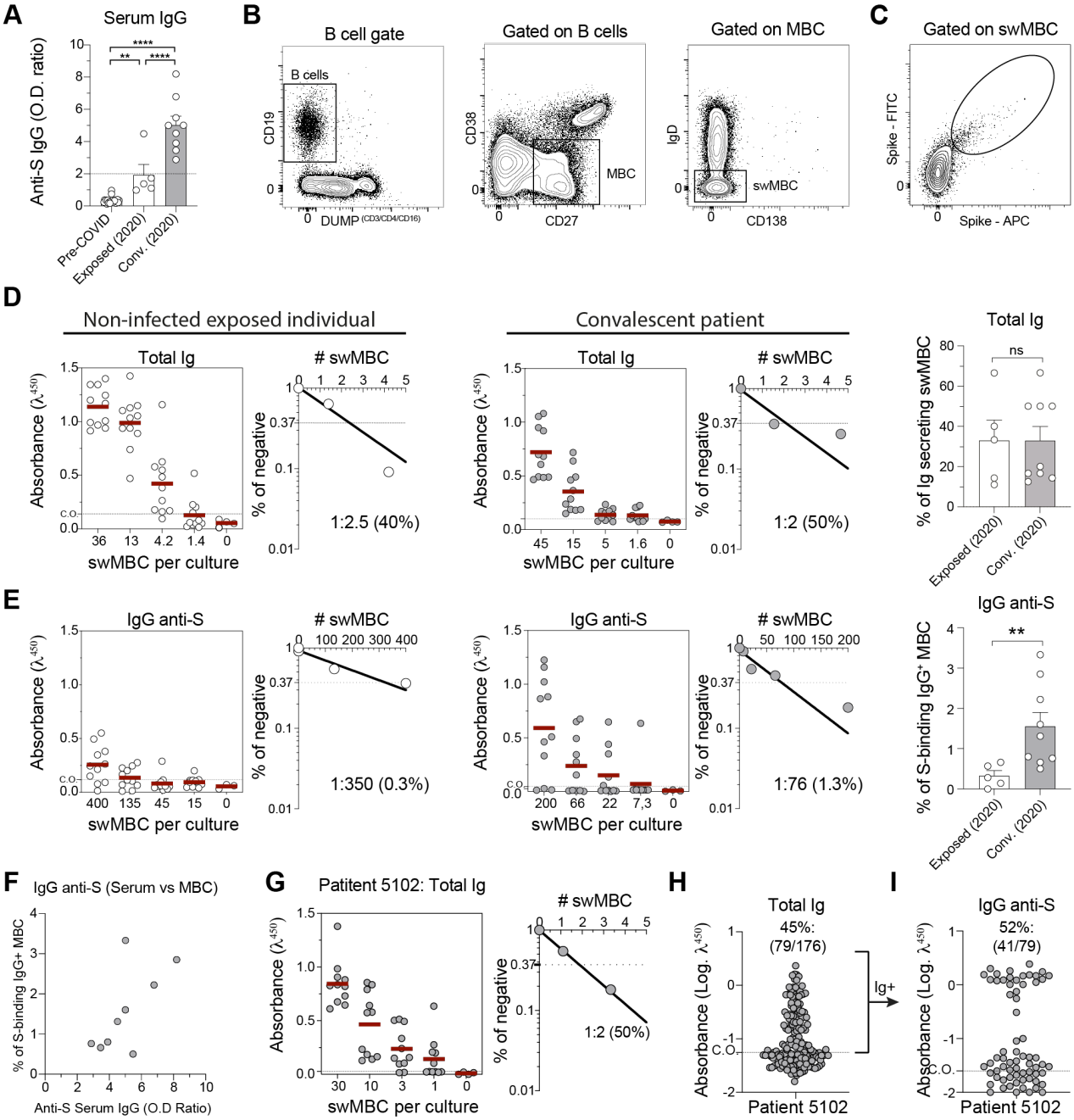

Fig. 1: Validation of a culture method for comprehensive and unbiased analysis of the human memory B cell (MBC) repertoire. (A) Serological analysis showing the optical density (OD) ratio of Spike-specific IgG in pre-COVID, SARS-CoV-2-exposed but PCR-negative ("exposed-negative"), and convalescent patients, assayed by ELISA. Statistical analyses were performed using one-way ANOVA followed by Tukey's multiple comparison test. **(B)** Gating strategy for sorting class switched MBCs (swMBCs). **(C)** Gating strategy for sorting Spike-baited swMBCs. **(D)** Limiting dilution assay (LDA) results from exposed-negative and convalescent patients, demonstrating the frequency of total Ig-secreting swMBC (representative donors shown on the left; pooled data shown in the dot plot). **(E)** Frequency of Spike-specific MBCs obtained from LDA culture of exposed-negative and convalescent patients (representative donors on the left; pooled data in the dot plot). Statistical analyses were performed using the unpaired two-tailed Student's t test. **(F)** Correlation between the OD ratio of Spike-specific IgG in serum and the

1336 frequency of Spike-specific MBCs measured by LDA. **(G)** LDA results from a
1337 convalescent patient 5102, showing the frequency of total Ig secreting swMBC
1338 (50%). **(H)** SCC of Spike-baited swMBCs from donor 5102, showing 45% Ig-
1339 secreting cells, closely matching the frequency obtained by LDA. **(I)** Frequency of
1340 Spike-specific swMBCs from donor 5102 obtained in SCC (52% specific to
1341 Wuhan Spike). Significant difference is indicated by asterisk (*, $P < 0.05$; **, $P <$
1342 0.01; (***, $P < 0.001$; ****, $P < 0.0001$). Error bars represent SEM.

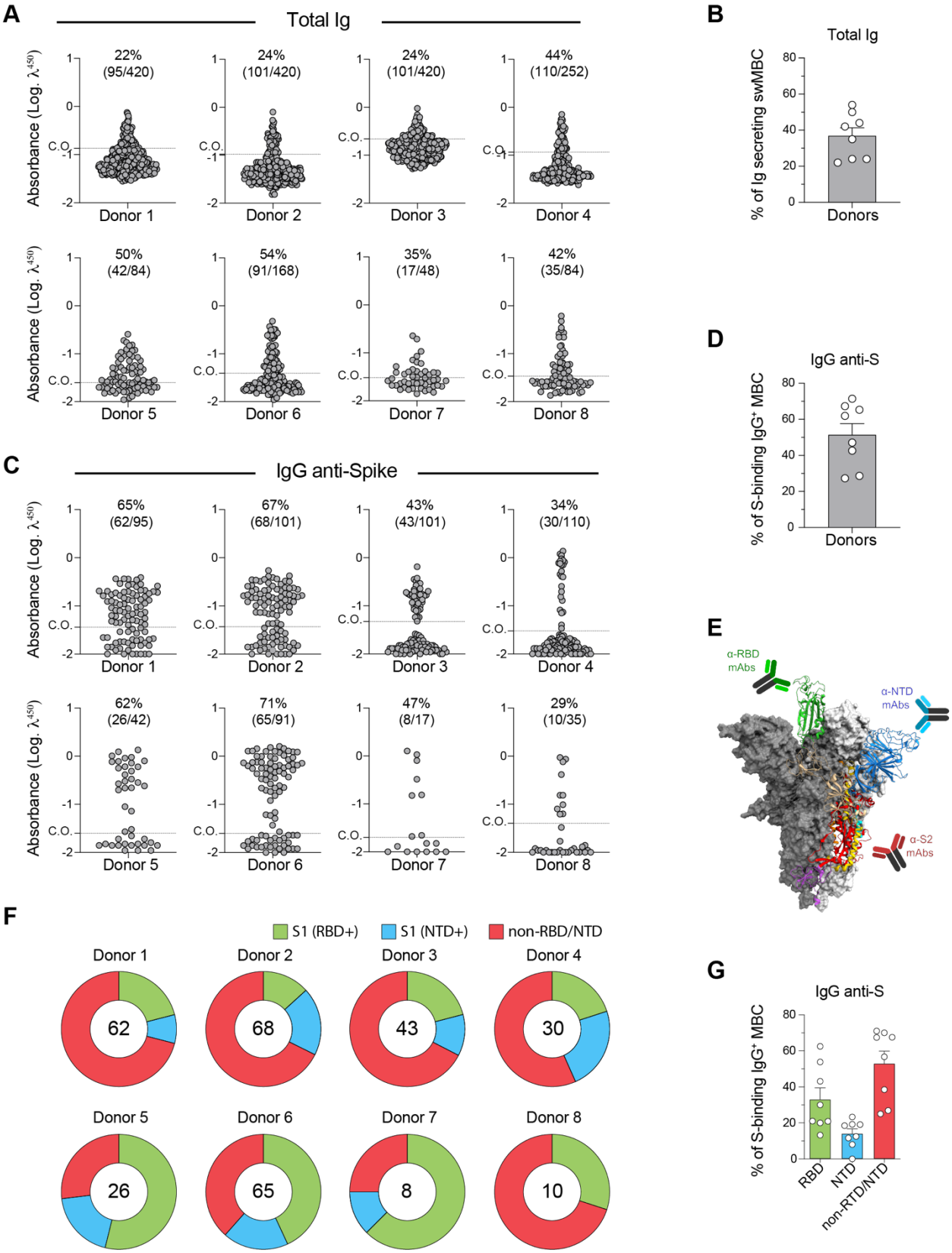

Fig. 2: Single-cell cultures (SCCs) for antigen-directed analysis of the Ig repertoire and monoclonal antibody (mAb) isolation. (A) Frequencies of antibody-producing cells in SCCs from eight vaccinated donors, ranging from 22% to 54%. **(B)** Pooled data showing frequencies of total Ig-secreting clones across donors. **(C)** Frequencies of mAbs binding to the Wuhan Spike protein, ranging from 29% to 71%. **(D)** Pooled data showing frequencies of Spike-specific clones across donors.

1350 **(E)** Schematic representation of the Spike protein regions, including the receptor-
1351 binding domain (RBD, green), N-terminal domain (NTD, blue), and S2 region
1352 (red). **(F)** Pie charts showing the distribution of mAbs targeting the RBD, NTD,
1353 and non-RBD/NTD (undefined) for each donor. **(G)** Pooled frequencies of
1354 domain-specific mAbs across donors. Error bars represent SEM.

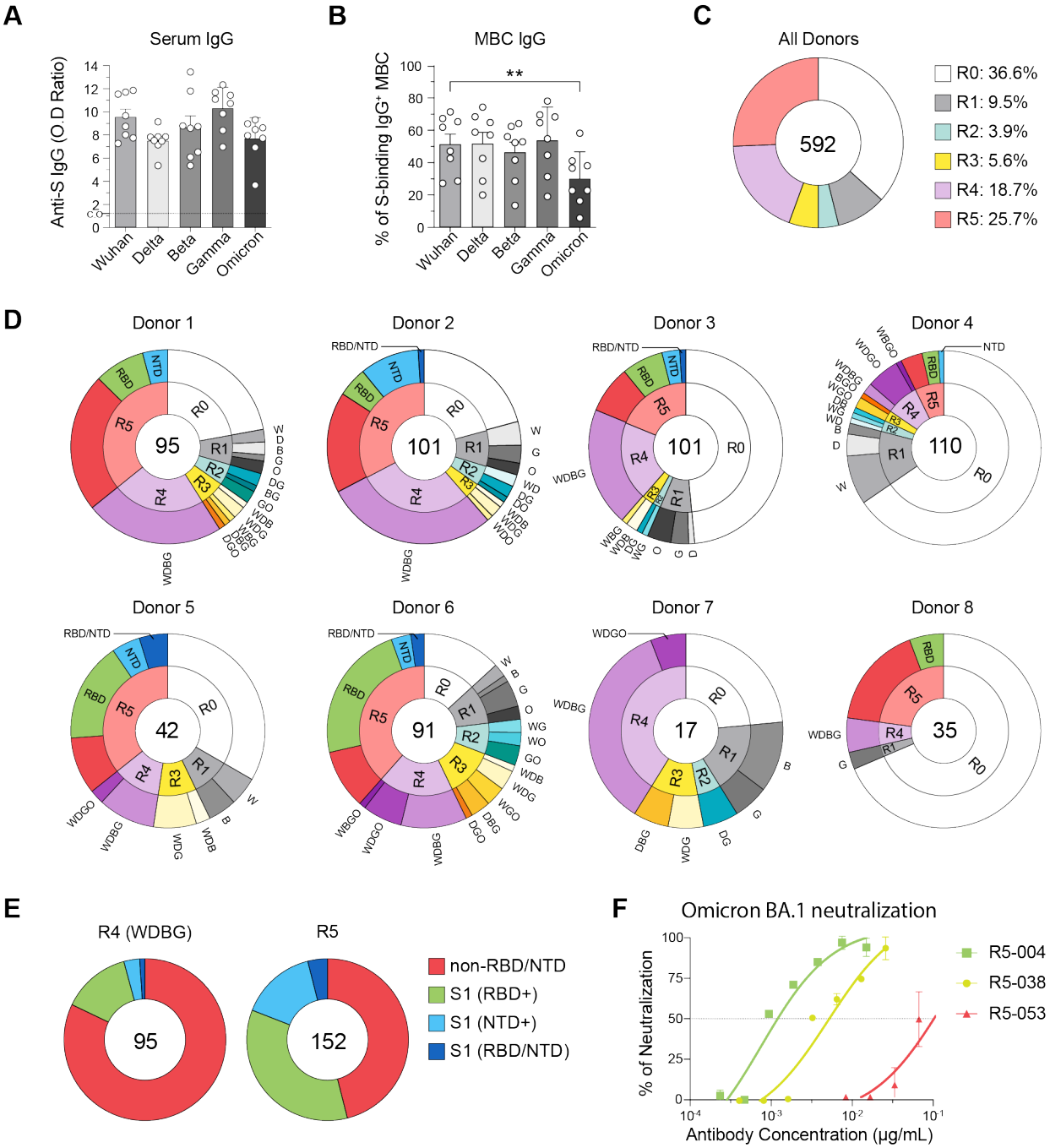

Fig. 3: Comparative cross-reactivity analysis of SCC-derived monoclonal antibodies (mAbs) against SARS-CoV-2 spike protein variants. (A) Serological analysis showing Spike-specific antibody responses against variants of concern (VOCs): Wuhan, Delta, Beta, Gamma, and Omicron (BA.2). **(B)** Frequency of IgG+ MBCs that recognized each VOC. S+ MBC cells were sorted, cultured and IgG production was assayed by ELISA. VOC reactivity was also measured by ELISA, through plates coated with Spike proteins from each variant. Statistical analyses were performed using one-way ANOVA, and Tukey's multiple comparison test. Significant difference is indicated by asterisk (**, $P < 0.01$) **(C)** Monoclonal antibodies isolated from the eight donors, stratified by cross-reactivity levels: R0 (no reactivity), R1 (reactivity to one variant), R2 (two variants), R3 (three variants), R4 (four variants), and R5 (reactivity to all five tested variants). **(D)** Cross-reactivity profiles for each of the eight donors, detailing the distribution of mAbs by cross-reactivity level and highlighting R5 mAbs, which are further

stratified by site-specific binding. R5 mAbs are emphasized due to their broader neutralizing potential. **(E)** Pie charts showing the proportions of R4 mAbs (excluding those non-reactive to Omicron, the most genetically divergent VOC) and R5 mAbs, categorized by specificity to the RBD, NTD, or undefined Spike regions (non-RBD/NTD). **(F)** Neutralizing activity of isolated R5 mAbs with site-specific binding to RBD (004 and 038) and putative S2-binding (053).

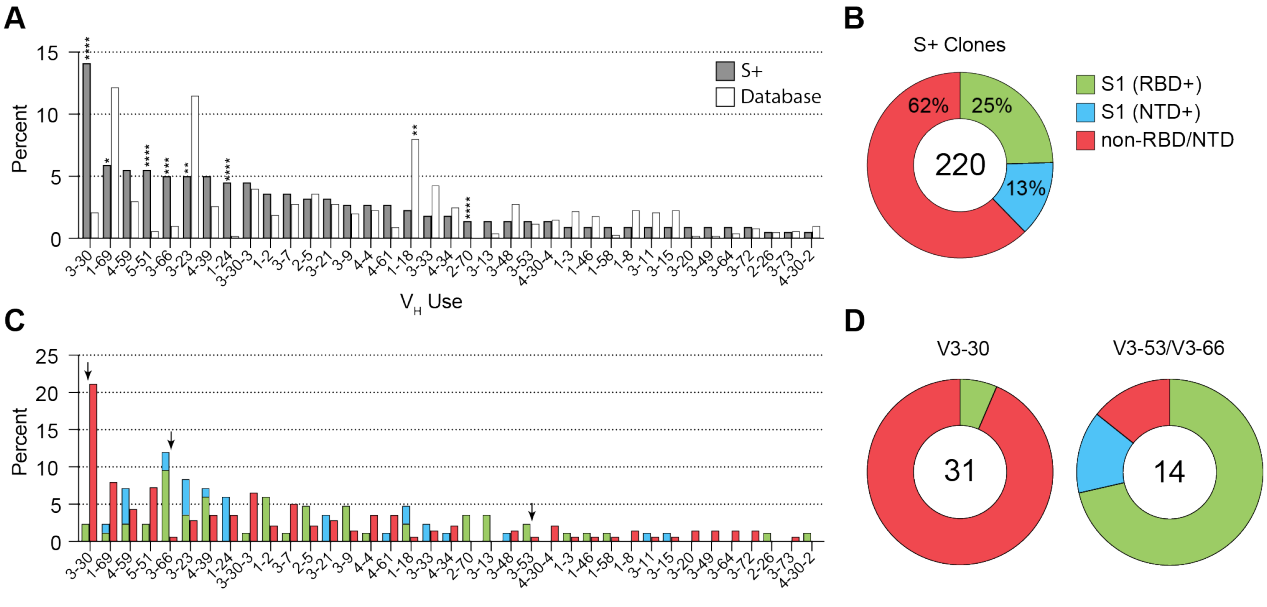

E

Representative convergent clones from different donors and independent datasets

		Heavy Chain					Light Chain					
Binding domain	**Clone ID**	IGHV	IGHD	IGHJ	CDR-H3	Length	IGKV-IGLV	IGKJ-IGLJ	CDR-L3	Length	*Cluster #	Source
RBD	22E1P1D02	IGHV3-66	IGHD2-2	IGHJ6	**ARDAQVYGMDV**	11	IGKV1-9	IGKJ4	**HQLNSDPPAT**	10	1 (RBD)	This study
	BD-503	IGHV3-53		IGHJ6	**ARDAAVYGIDV**	11	IGKV1-39	IGKJ3	**QQSYTTPLFT**	10		Cao et al, 2020
	22E1P1F08	IGHV3-66	IGHD3-9	IGHJ6	**ARDLVVSGMDV**	11	IGKV1-9	IGKJ4	**QQLNSDPLT**	9	1 (RBD)	This study
	C98C7	IGHV3-66	IGHD3-22	IGHJ6	**ARDLVVFGMDV**	11	IGKV3-20	IGKJ1	**QHYGSSP-T**	8		Tong et al, 2021
	23E1P2E01	IGHV1-58	IGHD2-15	IGHJ3	**AAPSCSGGSCYDGFNI**	16	IGKV3-20	IGKJ1	**QQYGGTTGWT**	10	3 (RBD)	This study
	MnC5t2p1_G1	IGHV1-58	IGHD2-15	IGHJ3	**AAPRCSGGSCYDGFDI**	16	IGKV3-20	IGKJ1	**QQYG-SSPWT**	9		Kreer et al, 2020
	CV3-1_	IGHV1-58	IGHD2-15	IGHJ3	**AAPSCSGGRCYDGFDI**	16	IGKV3-20	IGKJ1	**QQYG-TSPWT**	9		Jennewein et al, 2021
	23E1P1E11	IGHV3-66	IGHD3-10	IGHJ6	**ARDLMERGGMDV**	12	IGLV1-47	IGLJ2	**AAWDDTLSGRGV**	12	4 (RBD)	This study
	MOD9_P2_IgG_C9-P1369	IGHV3-66	IGHD2-15	IGHJ6	**ARDLMEVGGMDV**	12	IGLV1-47	IGLJ1	**AAWDDSLSG-YV**	12		Wang et al, 2021
Non-RBD/NTD Putative S2	22E1P4D02	IGHV3-30-3	IGHD4-23	IGHJ6	**ARATTGGYYYGMDV**	14	IGKV1-39	IGKJ2	**QQSYTTPYT**	9	6 (S2)	This study
	DH1202	IGHV3-30		IGHJ6	**ARAYSGGYYYGMDV**	14	IGKV1-39	IGKJ2	**QQSY-SLHS**	8		Li et al, 2021
	22E1P4B09	IGHV3-30-3	IGHD3-22	IGHJ6	**ARATRGSYYYGMDV**	14	IGKV1-39	IGKJ2	**QQGYSGPYT**	9	6 (S2)	This study
	DH1149	IGHV3-30		IGHJ6	**ARATRGSYYYGMDV**	14	IGKV1-39	IGKJ3	**QQSYSTEFT**	9		Li et al, 2021
	22E1P2E08	IGHV3-30	IGHD3-10	IGHJ4	**AKPGAANYYSSFDY**	14	IGKV3-20	IGKJ2	**QQYGSS--YT**	8	9 (S2)	This study
	ADI-60708	IGHV3-30	IGHD1-26	IGHJ4	**AKGYGGNYYSAFDY**	14	IGKV3D-15		**QQYNNWPPNT**	10		Sakharkar et al, 2021
	22E1P1B05	IGHV3-30	IGHD3-22	IGHJ4	**ARVRGGNYGGA-FDY**	14	IGLV3-21	IGLJ2	**QVWDRSG-DPDVV**	12	9 (S2)	This study
	COV2-2248	IGHV3-30	IGHD4-17	IGHJ4	**ARDSGGNYGDSYFDY**	15	IGLV3-25	IGLJ3	**QSVDRSGTYFNWV**	13		Zost et al, 2020
	22E1P3D10	IGHV4-59	NoD	IGHJ5	**ARGFDP**	6	IGKV3-20	IGKJ1	**HQYGSSLTWT**	10	10 (S2)	This study
	PDI_124	IGHV4-59		IGHJ5	**ARGFDP**	6	IGKV3-20	IGKJ1	**QQYGSSLRWT**	10		Wheatley et al, 2021
	22E1P3F12	IGHV3-7	IGHD6-13	IGHJ4	**ASLYSGSWNFDY**	12	IGLV3-1	IGLJ3	**QAWGSSTGV**	9	18 (S2)	This study
	COV2-2406	IGHV3-7	IGHD6-13	IGHJ4	**ARLGRSSWNFDY**	12	IGLV3-1	IGLJ3	**QAWDSSTGV**	9		Zost et al, 2020

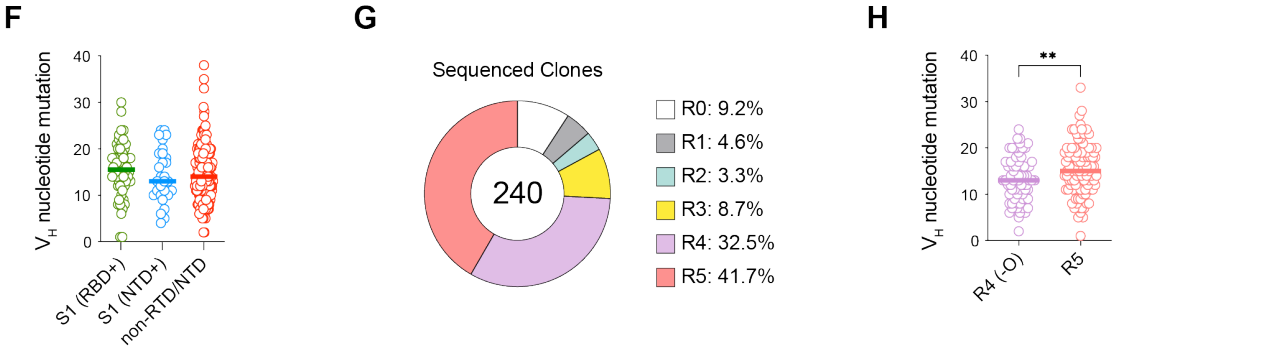

Fig.e 4: Immunoglobulin repertoire features and convergent V region rearrangements. (**A**) Frequency distribution of IGHV from clones isolated in the current study (gray bars) was compared to the frequency observed in healthy donor dataset (white bars). Statistical significance determined by two-sided binomial test with unequal variance. (**B**) Pie chart showing the percentage of S specific isolated antibodies that bind RBD, NTD or neither. The total number of antibodies tested is indicated at the center of the chart. RBD-/NTD- clones are likely to be S2 binding clones. (**C**) V_H usage distribution for clones that bind RBD, NTD or neither. (**D**) Pie charts displaying the percentage of RBD, NTD or non-RBD/NTD binding

clones in V3-30 or V3-53/ V3-66 clones. **(E)** Representative convergent antibody clusters. Clones that share 80% of CDRH3 identity as well as VH/VL usage with previously described clones that fall into clusters defined by Wang and colleagues. **(F)** Number of mutations detected in VH genes per clones that bind RBD, NTD or neither. **(G)** Pie chart with the total number of sequenced clones and the percentage distribution for VOC binding, from 0 variants (R0) to all five (R5). **(H)** Comparisons in V_H mutations detected per clones that bind four (R4, except Omicron) and five (R5) variants. Statistical analyses were performed using the unpaired two-tailed Student's t test. Significant differences are denoted by asterisks (*, $P < 0.05$; **, $P < 0.01$; ****, $P < 0.0001$).

A

Selected clones for scaleup production

		Heavy Chain					Light Chain				
Binding domain	**Clone ID**	IGHV	IGHJ	CDR-H3	Length	SHM	IGKV-IGLV	IGKJ-IGLJ	CDR-L3	Length	SHM
RBD	LBL01	IGHV3-53	IGHJ6	**ARGGGMGTYGMDV**	13	8	IGKV1-9	IGKJ3	**QHLDSYPQGFT**	11	2
	LBL02	IGHV3-66	IGHJ3	**ARDVADAFDI**	10	18	IGKV1-9	IGKJ2	**QQLNSYPPYT**	10	8

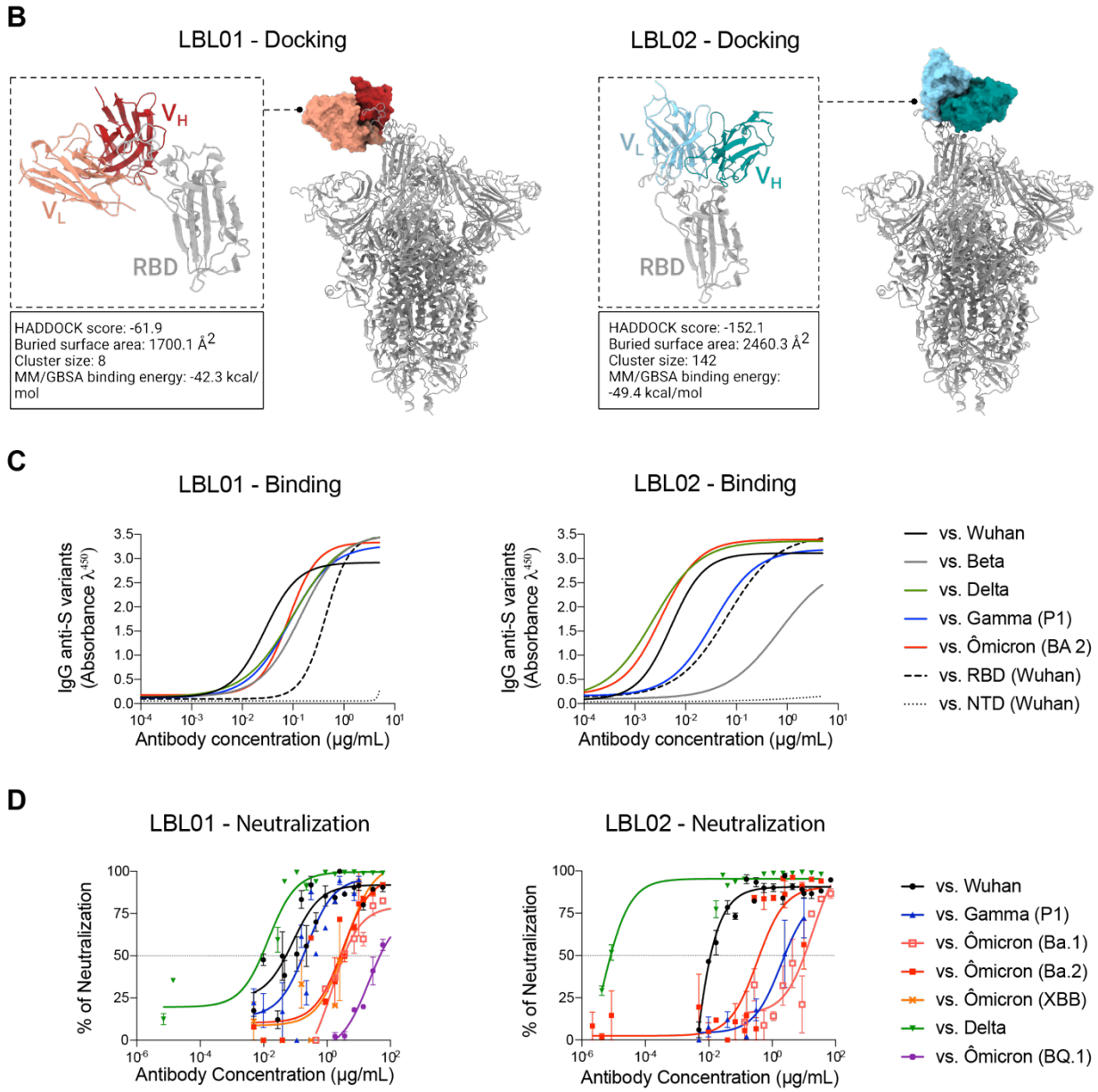

Fig. 5: Neutralizing potential of two selected RBD-targeting public clones. (A) Heavy and light chain CDR3 sequences of two public clones (LBL01 and LBL02) identified by ELISA as RBD binders. **(B)** Computational docking of each clone, showing the potential RBD binding site for each. **(C)** LBL01 and LBL02 antibodies were produced and tested in ELISA against five VOCs, as well as RBD and NTD domains . **(D)** Pseudovirus neutralization assay for both clones, confirming that the broader specificity of LBL02 is also functionally reflected in its stronger neutralization capability

Supplementary Materials for

Highly efficient and low-cost single-cell culture platform for unbiased analysis of human memory B cell repertoire and antibody discovery

Luciana Conde *et al.*

*Corresponding author. Email: valeam@biof.ufrj.br

This PDF file includes:

Figs. S1 to S6
Table S1

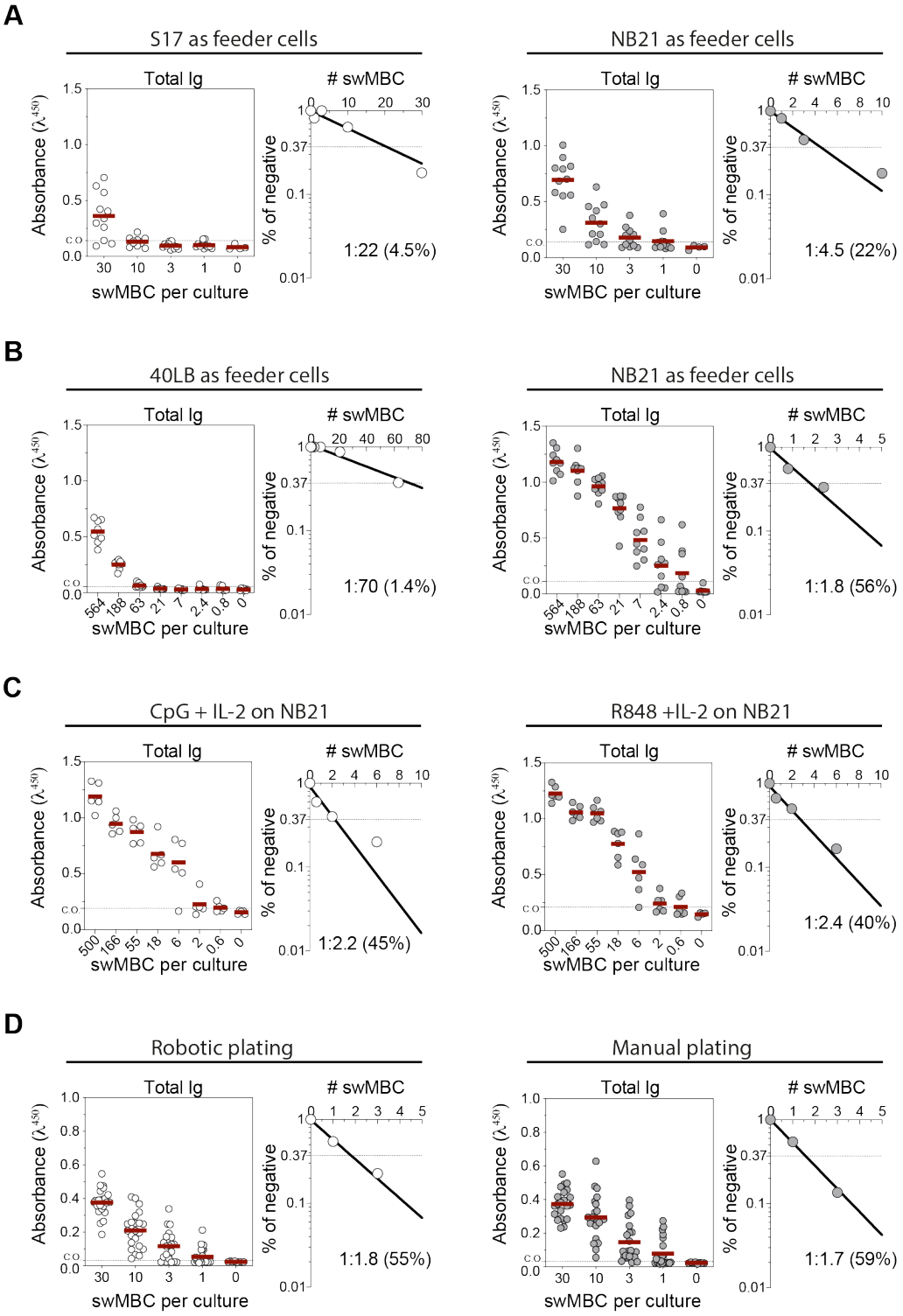

Fig. S1. Establishing effective culture conditions for *in vitro* expansion of human memory B cells.

(A) Frequency of responding MBCs co-cultured with S17 or NB21 feeder cells. **(B)** Frequency of responding MBCs co-cultured with 40LB or NB21 feeder cells. Decreasing number of B cells

were cultured and Ig secretion was assessed by ELISA. According to the Poisson distribution, the frequency of responding cells was calculated as the inverse of the cell density at which 37% of wells lacked detectable Ig (i.e., negative cultures). **(C)** Comparison of polyclonal stimuli efficacy using CpG and R848. **(D)** Comparison of responding cell frequencies obtained by manual plating versus automated robotic plating integrated into the sorting device.

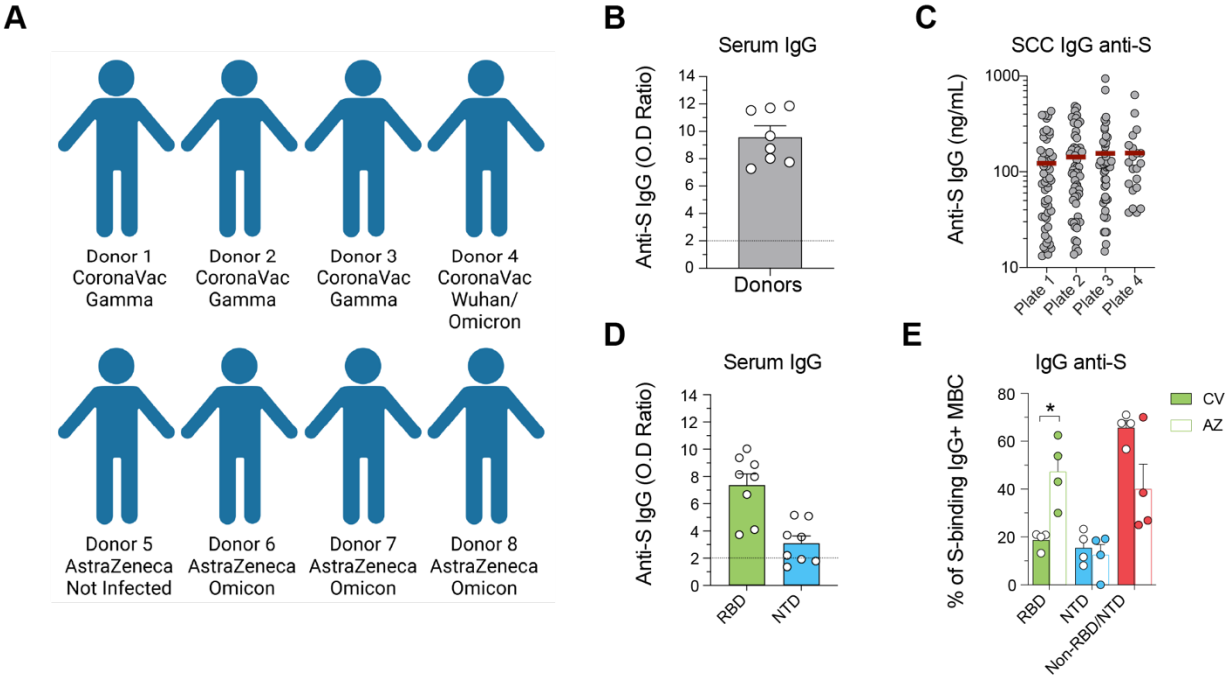

Fig. S2. Vaccination and infection history of patients used for monoclonal antibody isolation.

(A) Schematic representation of the vaccination and infection history for the eight donors from whom monoclonal antibodies were isolated. **(B)** OD (optical density) ratio of total IgG specific to the Spike protein in the serum of the eight donors. **(C)** Levels of anti-Spike IgG antibodies in SCC supernatants are expressed as ng/mL equivalents, quantified using a Wuhan anti-Spike human monoclonal antibody (CZmAb) as the standard. Four independent ELISA plates yielded average concentrations of 123 ng/mL, 143 ng/mL, 156 ng/mL, and 157 ng/mL of Spike-specific IgG. **(D)** OD ratio of IgG specific to the RBD and NTD regions in the serum of the eight donors. **(E)** Percentage of Spike-specific MBCs of each patient categorized by binding to the RBD, NTD, and undefined regions. Data are stratified by the type of vaccine administered to the patients: CoronaVac (CV), filled bars, or AstraZeneca (AZ), open bars. Statistical analyses were performed using the unpaired two-tailed Student's t test. Significant difference is indicated by asterisk (*, $P < 0.05$; **, $P < 0.01$; ***, $P < 0.001$; ****, $P < 0.0001$). Error bars represent SEM.

Fig. S3. Cross-reactivity levels of mAbs evaluated by ELISA.

Heatmap showing the binding intensity of monoclonal antibodies (mAbs) to variants of concern (VOCs) in ELISA assays. **(A)** R5 clones were ranked based on their OD (optical density) ratio values in the ELISA assay against Wuhan Spike and **(B)** Omicron Spike. Arrows indicate clones selected for pseudoneutralization assays.

A

ELISA-tested binding position: RBD

22E1P1D02
Binding domain: RBD
CDRH3 AA length and sequence:
11/ ARDAQVYGMDV
V gene usage: IGHV3-66/ IGKV1-9
127 structures in 12 cluster
Cluster size: 40
HADDOCK score: -96.4
Buried surface area: 2321.7 +/-112.4 Å^2
PRODIGY Predicted binding energy: -11.3 kcal/mol

22E1P1F08
Binding domain: RBD
CDRH3 AA length and sequence:
11/ ARDLVVSGMDV
V gene usage: IGHV3-66/ IGKV1-9
197 structures in 1 cluster
Cluster size: 197
HADDOCK score: -160.0
Buried surface area: 2301.6 +/- 17.3 Å^2
PRODIGY Predicted binding energy: -10.4 kcal/mol

B

Putative binding position: S2

22E1P3D10
Binding domain: S2
CDRH3 AA length and sequence:
6 / ARGFDP
V gene usage: IGHV4-59/ IGKV3-20
197 structures in 4 clusters
Cluster size: 152
HADDOCK score: -214.1
Buried surface area: 3754.5 +/- 67.3 Å^2
PRODIGY Predicted binding energy: -11.4 kcal/mol

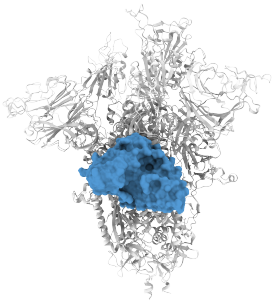

22E1P2E08
Binding domain: S2
CDRH3 AA length and sequence:
14/ AKPGAANYYSSFDY
V gene usage: IGHV3-30/ IGKV3-20
199 structures in 1 cluster
Cluster size: 199
HADDOCK score: -201.6
Buried surface area: 2571.6 +/- 59.2 Å^2
PRODIGY Predicted binding energy: -13.0 kcal/mol

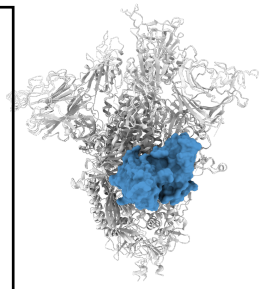

22E1P3F12
Binding domain: S2
CDRH3 AA length and sequence:
12/ ASLYSGSWNFDY
V gene usage: IGHV3-7/ IGLV3-1
199 structures in 1 cluster
Cluster size: 199
HADDOCK score: -147.7
Buried surface area: 2561.8 +/- 103.5 Å^2
PRODIGY Predicted binding energy: -11.2 kcal/mol

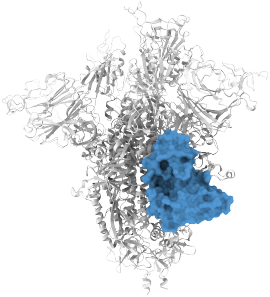

22E1P1B05
Binding domain: S2
CDRH3 AA length and sequence:
14/ ARVRGGNYGGAFDY
V gene usage: IGHV3-30/ IGLV3-21
179 structures in 5 clusters
Cluster size: 100
HADDOCK score: -180.7
Buried surface area: 2592.6 +/- 201.6 Å^2
PRODIGY Predicted binding energy: -8.0 kcal/mol

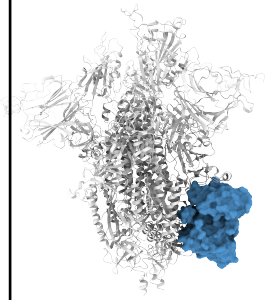

Fig. S4. *In silico* analysis of antibody binding.

(A) Driven docking data of the two selected RBD-binding clones. **(B)** Driven docking data of selected RBD-/NTD-, putative S2 binding clones, that shared CDRH3 sequence homology and V_H gene segments with clustered clones that are known to bind S2 domain.

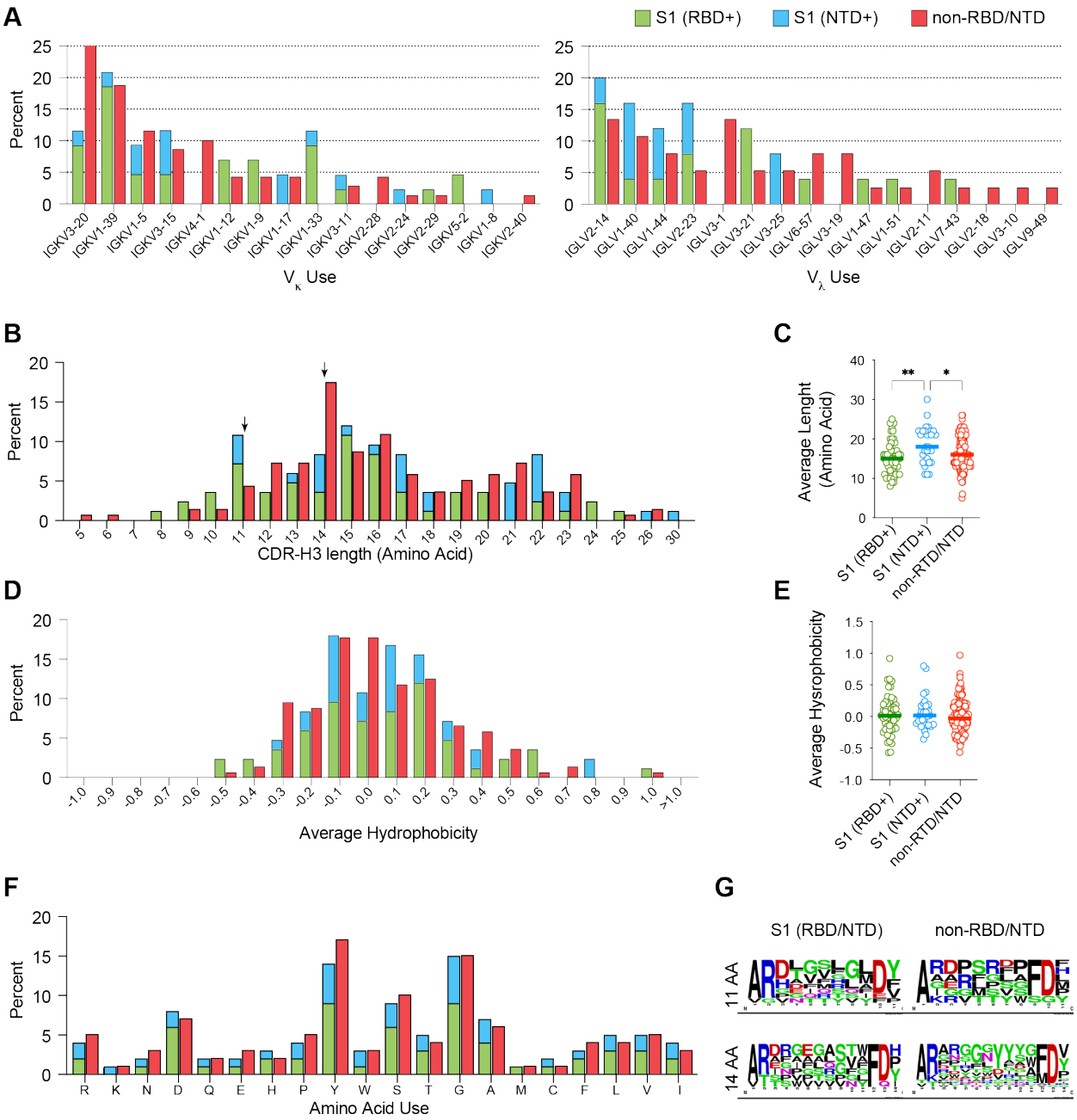

Fig. S5. IGKV and IGLV gene usage and CDR-H3 repertoire analysis.

(**A**) Distribution of CDRL3 V gene usage in κ and λ alleles for clones binding RBD, NTD, or RBD⁻/NTD⁻ Spike regions. **(B-C)** CDRH3 amino acid length distribution **(B)** and average length **(C)** for RBD, NTD or RBD-/NTD- S binding clones. Statistical analyses were performed using one-way ANOVA with Tukey's multiple comparison test. Significant difference is indicated by asterisk (*, $P < 0.05$; **, $P < 0.01$). **(D-E)** CDR-H3 average hydrophobicity index variation **(D)** and average hydrophobicity distribution **(E)** for RBD, NTD or RBD-/NTD- S binding clones. **(F)** Amino acid usage in CDRH3 of the assessed clones. **(G)** Logo plot of amino acid usage for clones binding RBD/NTD or neither, restricted to CDR-H3 loops of 11 or 14 amino acids.

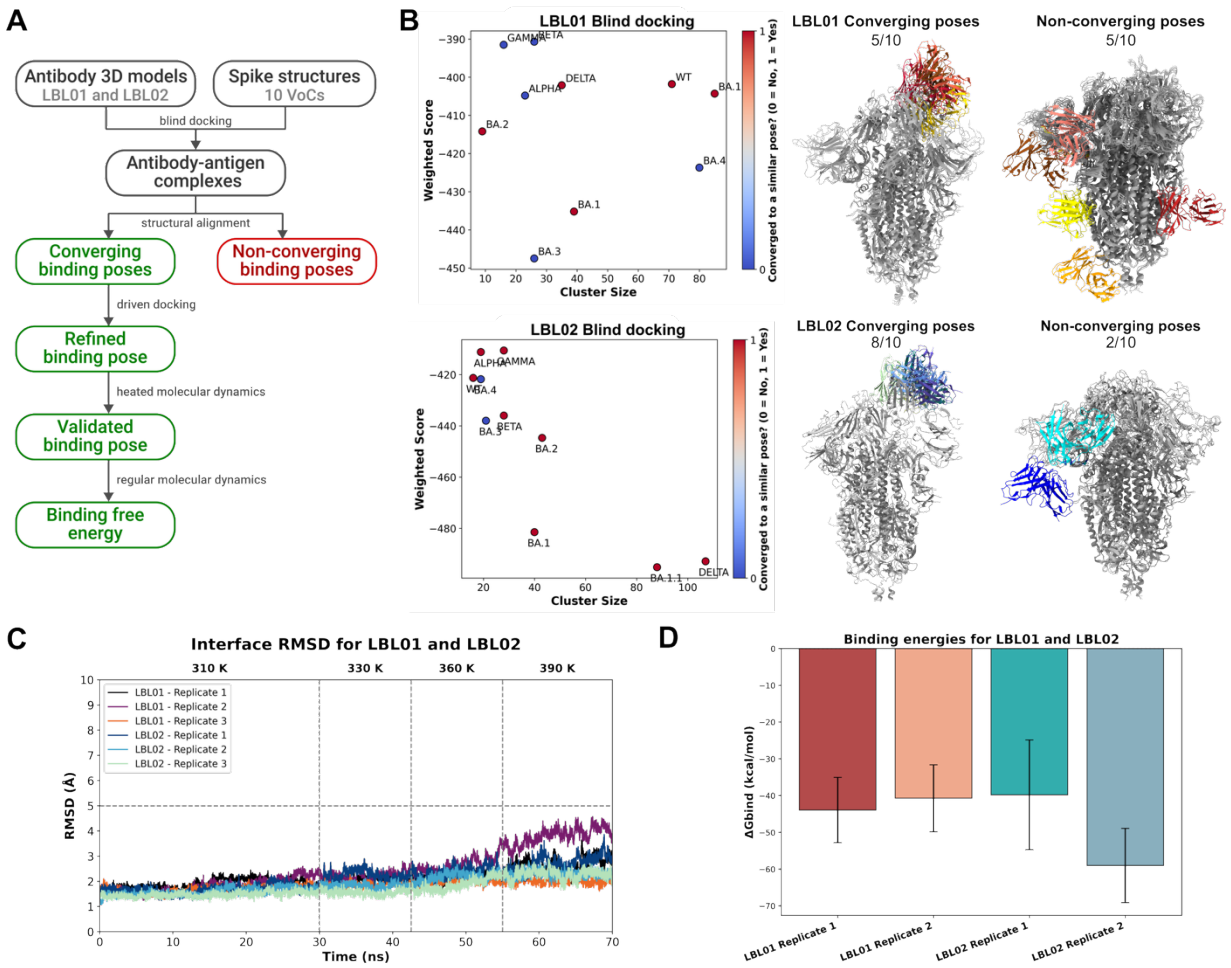

Fig. S6. LBL01 and LBL02 docking and molecular dynamics analysis.

(A) Computational workflow used to determine the binding poses and estimate the binding free energies of LBL01 and LBL02 with the Spike protein. **(B)** Blind docking of LBL01 and LBL02 with the Spike from 10 VOCs using ClusPro Antibody Mode compared in terms of cluster size and weighted score. Poses that converging to a similar region of Spike are shown in red, whereas the ones dispersed in other potential epitopes are in blue. Alignment of the docked complexes indicated that the converging poses bound to the RBD, suggesting a preferred binding mode. **(C)** Interface RMSD values of the antibody-RBD complexes during three independent replicates of heated MD simulations. A 5 Å cut-off was applied to identify stable binding poses, considered representative of true binding modes. **(D)** Binding free energy (ΔG_{bind}) of the LBL01 and LBL02 to RBD, obtained through MM/GBSA analysis of 150 ns MD simulations. More negative values indicate a more favorable interaction.

Supplementary Table 1: Summary of SCC cross-reactivity

Total SCCs per donor		Donor 1 (n = 420)		Donor 2 (n = 420)		Donor 3 (n = 420)		Donor 4 (n = 252)		Donor 5 (n = 84)		Donor 6 (n =168)		Donor 7 (n =48)		Donor 8 (n =84)		Total (n=1896)	
Immunoreactivity		#	%	#	%	#	%	#	%	#	%	#	%	#	%	#	%	#	%
Total Ig secreting SCCs		95	100.0	101	100.0	101	100.0	110	100.0	42	100.0	91	100.0	17	100.0	35	100.0	592	100.0
Spike +	**Wuhan (W)**	62	65.3	68	67.3	43	42.6	30	27.3	26	61.9	65	71.4	8	47.1	10	28.6	312	52.7
Spike region	RBD (W)	13	21.0	9	13.2	9	20.9	6	20.0	14	53.8	28	43.1	5	62.5	3	30.0	87	27.9
	NTD (W)	5	8.1	13	19.1	5	11.6	7	23.3	5	19.2	12	18.5	1	12.5	0	0.0	48	15.4
	non-RBD/NTD	44	71.0	46	67.6	29	67.4	17	56.7	7	26.9	25	38.5	2	25.0	7	70.0	177	56.7
VOCs	**Delta (D)**	65	68.4	75	74.3	43	42.6	22	20.0	24	57.1	59	64.8	10	58.8	10	28.6	308	52.0
	Beta (B)	61	64.2	63	62.4	42	41.6	15	13.6	22	52.4	51	56.0	9	52.9	10	28.6	273	46.1
	Gamma G)	66	69.5	69	68.3	45	44.6	21	19.1	23	54.8	71	78.0	11	64.7	11	31.4	317	53.5
	Omicron (O)	39	41.1	37	36.6	23	22.8	18	16.4	16	38.1	53	58.2	1	5.9	8	22.9	195	32.9
Cross-reactivity level																			
R0		21	22.1	21	20.8	49	48.5	72	65.5	14	33.3	12	13.2	4	23.5	24	68.6	217	36.7
R1, R2, R3, R4, R5		74	77.9	80	79.2	52	51.5	38	34.5	28	66.7	79	86.8	13	76.5	11	31.4	375	63.3
R1		7	7.4	9	8.9	8	7.9	15	13.6	4	9.5	9	9.9	3	17.6	1	2.9	56	9.5
R1: VOCs	**W**	2	2.1	0	0.0	0	0.0	9	8.2	2	4.8	2	2.2	0	0.0	0	0.0	15	2.5
	D	2	2.1	4	4.0	1	1.0	4	3.6	0	0.0	0	0.0	0	0.0	0	0.0	11	1.9
	B	1	1.1	0	0.0	0	0.0	2	1.8	2	4.8	1	1.1	2	11.8	0	0.0	8	1.4
	G	0	0.0	3	3.0	3	3.0	0	0.0	0	0.0	4	4.4	1	5.9	1	2.9	12	2.0
	O	2	2.1	2	2.0	4	4.0	0	0.0	0	0.0	2	2.2	0	0.0	0	0.0	10	1.7
R2		5	5.3	5	5.0	2	2.0	3	2.7	0	0.0	7	7.7	1	5.9	0	0.0	23	3.9
R2: VOC combinations	**WD**	0	0.0	2	2.0	0	0.0	1	0.9	0	0.0	0	0.0	0	0.0	0	0.0	3	0.5
	WB	0	0.0	0	0.0	0	0.0	0	0.0	0	0.0	0	0.0	0	0.0	0	0.0	0	0.0
	WG	0	0.0	0	0.0	1	1.0	1	0.9	0	0.0	2	2.2	0	0.0	0	0.0	4	0.7
	WO	0	0.0	0	0.0	0	0.0	0	0.0	0	0.0	2	2.2	0	0.0	0	0.0	2	0.3
	DB	0	0.0	0	0.0	0	0.0	1	0.9	0	0.0	0	0.0	0	0.0	0	0.0	1	0.2
	DG	2	2.1	2	2.0	1	1.0	0	0.0	0	0.0	0	0.0	1	5.9	0	0.0	6	1.0
	DO	0	0.0	1	1.0	0	0.0	0	0.0	0	0.0	0	0.0	0	0.0	0	0.0	1	0.2
	BG	1	1.1	0	0.0	0	0.0	0	0.0	0	0.0	0	0.0	0	0.0	0	0.0	1	0.2
	BO	0	0.0	0	0.0	0	0.0	0	0.0	0	0.0	0	0.0	0	0.0	0	0.0	0	0.0
	GO	2	2.1	0	0.0	0	0.0	0	0.0	0	0.0	3	3.3	0	0.0	0	0.0	5	0.8
R3		6	6.3	4	4.0	3	3.0	3	2.7	4	9.5	11	12.1	2	11.8	0	0.0	33	5.6
R3: VOC combinations	**WDB**	1	1.1	1	1.0	2	2.0	0	0.0	1	2.4	1	1.1	0	0.0	0	0.0	6	1.0
	WDG	2	2.1	2	2.0	0	0.0	0	0.0	3	7.1	3	3.3	1	5.9	0	0.0	11	1.9
	WDO	0	0.0	1	1.0	0	0.0	0	0.0	0	0.0	0	0.0	0	0.0	0	0.0	1	0.2
	WBG	1	1.1	0	0.0	1	1.0	0	0.0	0	0.0	0	0.0	0	0.0	0	0.0	2	0.3
	WBO	0	0.0	0	0.0	0	0.0	0	0.0	0	0.0	0	0.0	0	0.0	0	0.0	0	0.0
	WGO	0	0.0	0	0.0	0	0.0	2	1.8	0	0.0	3	3.3	0	0.0	0	0.0	5	0.8
	DBG	1	1.1	0	0.0	0	0.0	0	0.0	0	0.0	3	3.3	1	5.9	0	0.0	5	0.8
	DBO	0	0.0	0	0.0	0	0.0	0	0.0	0	0.0	0	0.0	0	0.0	0	0.0	0	0.0
	DGO	1	1.1	0	0.0	0	0.0	0	0.0	0	0.0	1	1.1	0	0.0	0	0.0	2	0.3
	BGO	0	0.0	0	0.0	0	0.0	1	0.9	0	0.0	0	0.0	0	0.0	0	0.0	1	0.2
R4		22	23.2	29	28.7	20	19.8	9	8.2	5	11.9	17	18.7	7	41.2	2	5.7	111	18.8
R4: VOC combinations	**WDBG**	22	23.2	29	28.7	20	19.8	2	1.8	4	9.5	10	11.0	6	35.3	2	5.7	95	16.0
	WDBO	0	0.0	0	0.0	0	0.0	0	0.0	0	0.0	0	0.0	0	0.0	0	0.0	0	0.0
	WDGO	0	0.0	0	0.0	0	0.0	6	5.5	1	2.4	6	6.6	1	5.9	0	0.0	14	2.4
	WBGO	0	0.0	0	0.0	0	0.0	1	0.9	0	0.0	1	1.1	0	0.0	0	0.0	2	0.3
	DBGO	0	0.0	0	0.0	0	0.0	0	0.0	0	0.0	0	0.0	0	0.0	0	0.0	0	0.0
R5		34	35.8	33	32.7	19	18.8	8	7.3	15	35.7	35	38.5	0	0.0	8	22.9	152	25.7
Spike region	**non-RBD/NTD**	22	23.2	17	16.8	8	7.9	4	3.6	4	9.5	9	9.9	0	0.0	6	17.1	70	11.8
	RBD+	8	8.4	5	5.0	7	6.9	3	2.7	7	16.7	21	23.1	0	0.0	2	5.7	53	9.0
	NTD+	4	4.2	10	9.9	3	3.0	1	0.9	2	4.8	3	3.3	0	0.0	0	0.0	23	3.9
	RBD/NTD	0	0.0	1	1.0	1	1.0	0	0.0	2	4.8	2	2.2	0	0.0	0	0.0	6	1.0

Table S1. Summary of site-specific and cross-reactive single cell cloning cultures.